

Up-regulated Ectonucleotidases in Fas-Associated Death Domain Protein– and Receptor-Interacting Protein Kinase 1–Deficient Jurkat Leukemia Cells Counteract Extracellular ATP/AMP Accumulation via Pannexin-1 Channels during Chemotherapeutic Drug-Induced Apoptosis

Andrea M. Boyd-Tressler, Graham S. Lane, and George R. Dubyak

Department of Physiology & Biophysics (G.S.L., G.R.D.), Department of Pharmacology (A.M.B.-T., G.R.D.), and Case Comprehensive Cancer Center (G.R.D.), School of Medicine, Case Western Reserve University, Cleveland, Ohio

Received February 23, 2016; accepted April 26, 2017

ABSTRACT

Pannexin-1 (Panx1) channels mediate the efflux of ATP and AMP from cancer cells in response to induction of extrinsic apoptosis by death receptors or intrinsic apoptosis by chemotherapeutic agents. We previously described the accumulation of extracellular ATP/AMP during chemotherapy-induced apoptosis in Jurkat human leukemia cells. In this study, we compared how different signaling pathways determine extracellular nucleotide pools in control Jurkat cells versus Jurkat lines that lack the Fas-associated death domain (FADD) or receptor-interacting protein kinase 1 (RIP1) cell death regulatory proteins. Tumor necrosis factor- α induced extrinsic apoptosis in control Jurkat cells and necroptosis in FADD-deficient cells; treatment of both lines with chemotherapeutic drugs elicited similar intrinsic apoptosis. Robust extracellular ATP/AMP accumulation was observed in the FADD-deficient cells during necroptosis, but not during apoptotic activation of Panx1 channels. Accumulation of extracellular ATP/AMP was similarly absent in RIP1-deficient Jurkat

cells during apoptotic responses to chemotherapeutic agents. Apoptotic activation triggered equivalent proteolytic gating of Panx1 channels in all three Jurkat cell lines. The differences in extracellular ATP/AMP accumulation correlated with cell-line-specific expression of ectonucleotidases that metabolized the released ATP/AMP. CD73 mRNA, and α,β -methylene-ADP-inhibitable ecto-AMPase activity were elevated in the FADD-deficient cells. In contrast, the RIP1-deficient cells were defined by increased expression of tartrate-sensitive prostatic acid phosphatase as a broadly acting ectonucleotidase. Thus, extracellular nucleotide accumulation during regulated tumor cell death involves interplay between ATP/AMP efflux pathways and different cell-autonomous ectonucleotidases. Differential expression of particular ectonucleotidases in tumor cell variants will determine whether chemotherapy-induced activation of Panx1 channels drives accumulation of immunostimulatory ATP versus immunosuppressive adenosine within the tumor microenvironment.

Introduction

The efficacy of cancer chemotherapy is enhanced by induction of sustainable antitumor immune responses. This is determined in part by accumulation of immunogenic mediators

within the tumor microenvironment. These include bioactive peptides, lipids, and nucleotides released from cancer cells during chemotherapy- or receptor-induced activation of cell death signaling responses (Gude et al., 2008; Peter et al., 2008, 2012; Truman et al., 2008; Zitvogel et al., 2008; Ghiringhelli et al., 2009; Kepp et al., 2009; Vacchelli et al., 2015). Given its high intracellular concentration, ATP comprises a ubiquitous tumor cell-derived immunogenic mediator. Extracellular ATP acts as a “find-me” signal for G protein-coupled P2Y-family

This work was supported by grants from the National Institutes of Health Institute of General Medical Sciences [grants R01-GM36387 and T32-GM00803] and National Eye Institute [R01-EY014362].
<https://doi.org/10.1124/mol.116.104000>.

ABBREVIATIONS: APCP, α,β -methylene-adenosine 5'-diphosphate; ARL-67156, [dibromo-[[[(2R,3S,4R,5R)-5-[6-(diethylamino)purin-9-yl]-3,4-dihydroxoxolan-2-yl]methoxy-hydroxyphosphoryl]oxy-hydroxyphosphoryl]methyl]phosphonic acid; BSA, bovine serum albumin; BSS, basal salt solution; BV6, (2S)-1-[[[(2S)-2-cyclohexyl-2-[[[(2S)-2-(methylamino)propanoyl]amino]acetyl]-N-[[[(2S)-1-[6-[[[(2S)-2-[[[(2S)-1-[[[(2S)-2-cyclohexyl-2-[[[(2S)-2-(methylamino)propanoyl]amino]acetyl]pyrrolidine-2-carbonyl]amino]-3,3-diphenylpropanoyl]amino]hexylamino]-1-oxo-3,3-diphenylpropan-2-yl]pyrrolidine-2-carboxamide; cIAP, cytosolic inhibitor of apoptosis; DAPI, 4',6-diamidino-2-phenylindole; ϵ -ADO, etheno-adenosine; ϵ -AMP, 1, N⁶-etheno-AMP; Etop, etoposide; FADD, Fas-associated death domain protein; FLAAB, firefly Luciferase ATP assay Buffer; FLAAM, lyophilized firefly Luciferase ATP assay mix; HPLC, high-pressure liquid chromatography; LDH, lactate dehydrogenase; MLKL, mixed lineage kinase-like protein; NSA, necrosulfonamide; Panx1, pannexin-1; PAP, prostatic acid phosphatase; PARP, poly(ADP-ribose) polymerase; PBS, phosphate-buffered saline; qRT-PCR, quantitative reverse-transcription polymerase chain reaction; RIP, receptor-interacting protein kinase; Smac, second mitochondrial-derived activator of apoptosis; STS, staurosporine; Tetra, tetramisole; TM-PAP, prostatic acid phosphatase, transmembrane splice variant; TNAP, tissue nonselective alkaline phosphatase; TNF, tumor necrosis factor; TNFR, tumor necrosis factor receptor; TRAIL, TNF-related apoptosis-inducing ligand; Trova, trovafloxacin; WT, wild type; zVAD-fmk, benzyloxycarbonyl-Val-Ala-dl-Asp(O-methyl)-fluoromethylketone.

receptors expressed on nearby macrophages and dendritic cells (Elliott et al., 2009; Chekeni et al., 2010; Ma et al., 2013). This amplifies chemotaxis of these phagocytic leukocytes to the vicinity of dying cells and thereby facilitates the phagocytosis of tumor cells required for processing and presentation of tumor antigens to T lymphocytes.

Pannexin-1 (Panx1) channels comprise a major pathway for the regulated release of ATP to extracellular compartments in response to induction of either extrinsic apoptosis by death receptors or intrinsic apoptosis by chemotherapeutic agents (Chekeni et al., 2010; Boyd-Tressler et al., 2014). Apoptotic induction of active caspase-3 results in proteolytic excision of an autoinhibitory C-terminal segment to drive open gating of the large-pore Panx1 channels and consequent efflux of intracellular metabolites such as ATP (Chekeni et al., 2010; Sandilos et al., 2012; Boyd-Tressler et al., 2014).

Several therapeutic agents, including agonists for tumor necrosis factor (TNF)/TNF-related apoptosis-inducing ligand (TRAIL) family death receptors and various chemotherapeutic drugs, may induce regulated cancer cell death either by apoptosis or by necroptosis (Martinou and Youle, 2011; Humphries et al., 2015). The latter involves formation of necrosome complexes between RIP1 and RIP3 (receptor interacting protein kinases 1 and 3) to drive RIP3-mediated phosphorylation of the mixed-lineage kinase like (MLKL) pseudo-kinase. Phosphorylated mixed lineage kinase-like (pMLKL) protein oligomerizes and inserts into the plasma membrane as multimeric pores with significant permeability to organic metabolites such as ATP (Sun et al., 2012; Su et al., 2014; Wang et al., 2014, 2015; Humphries et al., 2015). However, the relative kinetics and magnitudes of extracellular ATP accumulation as mediated by RIP3-activated MLKL pores versus caspase-3-activated Panx1 channels in a given tumor cell model have not been quantified and compared.

Intrinsic apoptosis, extrinsic apoptosis, and necroptosis share several signaling nodes and regulatory proteins (Fig. 1A). TNF- α binding to type 1 TNF receptors (TNFR1) induces formation of “complex 1” containing the TNF receptor-associated death domain protein adapter, RIP1, and cIAP1/2 (cytosolic inhibitor of apoptosis proteins 1 and 2). This elicits nuclear factor κ B signaling and cell survival. However, when mitochondria release second mitochondrial-derived activator of apoptosis (Smac) protein or when cells are treated with Smac-mimetic drugs, the cIAPs are down-regulated to facilitate the assembly of “complex 2,” containing RIP1, FADD (Fas-associated death domain) adapter, and caspase-8. Under these conditions, caspase-8 is activated to both initiate apoptosis and inactivate RIP1. However, if cells lacking FADD are treated with TNF- α and Smac-mimetic, complex 2 cannot assemble, leaving RIP1 free to drive the RIP3/MLKL necroptotic cascade.

Riptosome signaling complexes, like “complex 2” platforms, contain RIP1, FADD, and procaspase-8, but also cFLIP, cellular FLICE-inhibitory protein (cFLIP), a protease-inactive caspase-8-like modulator protein. Although FADD is best characterized for its roles in extrinsic apoptosis, the assembly of riptosomes can amplify death signaling by chemotherapeutic drugs that induce intrinsic apoptosis due to release of mitochondrial Smac and down-regulation of cIAPs (Feoktistova et al., 2011; Tenev et al., 2011; Belz et al., 2014).

Although ATP directly released from dying tumor cells supports immunogenic antitumor responses by stimulating

P2Y receptor signaling, it can also drive the generation of adenosine, which activates immunosuppressive A_{2A}/A_{2B} receptors expressed on immune cells (Stagg and Smyth, 2010; Antonioli et al., 2013a). The balance between local ATP and adenosine accumulation within the tumor microenvironment can determine the net efficacy of anticancer immunogenic responses. Multiple studies have linked the decreased efficacy of cancer chemotherapies to increased levels of ectonucleotidases that metabolize released adenine nucleotides to adenosine (Mikhailov et al., 2008; Beavis et al., 2012; Loi et al., 2013). A wide range of ectoenzymes may differentially contribute to interstitial adenine nucleotide and adenosine levels in particular tumor environments (Table 1).

In this study, we compared how alternative pathways of nucleotide efflux and ectometabolism determine the composition of extracellular adenine nucleotide pools during death receptor-induced apoptosis or necroptosis versus chemotherapeutic drug-induced apoptosis in control Jurkat cells versus Jurkat variants lacking the FADD adapter protein or RIP1 kinase that modulate apoptotic and necroptotic cell death signaling responses.

Materials and Methods

Cell Models and Reagents. The FADD-deficient human Jurkat T-cell acute leukemia cell line (I 2.1) and the wild-type (WT) human Jurkat T-cell acute leukemia cells were obtained from the American Type Culture Collection (Manassas VA). The RIP1-deficient human Jurkat T-cell acute leukemia cell line was generously provided by Zheng-gang Liu (National Cancer Institute, Bethesda MD) (Morgan et al., 2009). BV6 [(2S)-1-[(2S)-2-cyclohexyl-2-[(2S)-2-(methylamino)propanoyl]amino]acetyl]-N-[(2S)-1-[6-[(2S)-2-[(2S)-1-[(2S)-2-cyclohexyl-2-[(2S)-2-(methylamino)propanoyl]amino]acetyl]pyrrolidine-2-carbonyl]amino]-3,3-diphenylpropanoyl]amino]hexylamino]-1-oxo-3,3-diphenylpropan-2-yl]pyrrolidine-2-carboxamide] was provided by Genentech (South San Francisco, CA). Other key reagents were purchased from commercial vendors. Human recombinant TNF- α was obtained from PeproTech (Rocky Hill, NJ). Benzoyloxycarbonyl-Val-Ala-dl-Asp(O-methyl)-fluoromethylketone (zVAD-fmk) and pentostatin (2-deoxycoformycin) were from APEXBio (Houston, TX). Necrosulfonamide (NSA) and ARL-67156 ([dibromo-[[[(2R,3S,4R,5R)-5-[6-(diethylamino)purin-9-yl]-3,4-dihydroxyoxolan-2-yl]methoxy-hydroxyphosphoryl]oxy-hydroxyphosphoryl]methyl]phosphonic acid) were obtained from Tocris (Minneapolis, MN). Anti-human Fas (CH11 clone) was obtained from Millipore (Billerica MA). Staurosporine was from LC Laboratories (Woburn, MA). Lyophilized firefly luciferase ATP assay mix (FLAAM), firefly luciferase ATP assay buffer (FLAAB), pyruvate kinase (P-1506), myokinase (M-3003), ATP, 1,N⁶-etheno-AMP (ϵ -AMP), phosphoenolpyruvate, etoposide, tetramisole, trovafloxacin, L-tartaric acid (Na salt), TRIZOL reagent, amphotericin B, and 4',6-diamidino-2-phenylindole (DAPI) stain were obtained from Sigma-Adrich (St. Louis, MO). Calcein-AM, YO-PRO (green fluorescent stain), and MitoTracker Red CM-H₂XRos were obtained from Invitrogen (Carlsbad, CA). The cytotoxicity detection kit (lactate dehydrogenase [LDH] release) was purchased from Roche Applied Science (Indianapolis, IN). Anti-poly(ADP-ribose) polymerase (PARP) (9542) was purchased from Cell Signaling Technology (Danvers, MA). Anti-prostatic acid phosphatase (PAP) was from R&D Systems (Minneapolis, MN). All-in-One FirstStrand cDNA Synthesis Kit, All-in-One qPCR Mix, CD73 real-time quantitative reverse-transcription polymerase chain reaction (qRT-PCR) primers, and GAPDH qRT-PCR primers were obtained from GeneCopoeia (Rockville, MD). Anti- β actin (sc-1615) and all horseradish peroxidase-coupled secondary antibodies were from Santa Cruz Biotechnology (Dallas, TX). Pierce electrochemiluminescence Western blotting substrate was obtained from ThermoFisher Scientific (Waltham, MA). The $\alpha\beta$ -methylene-adenosine 5'-diphosphate

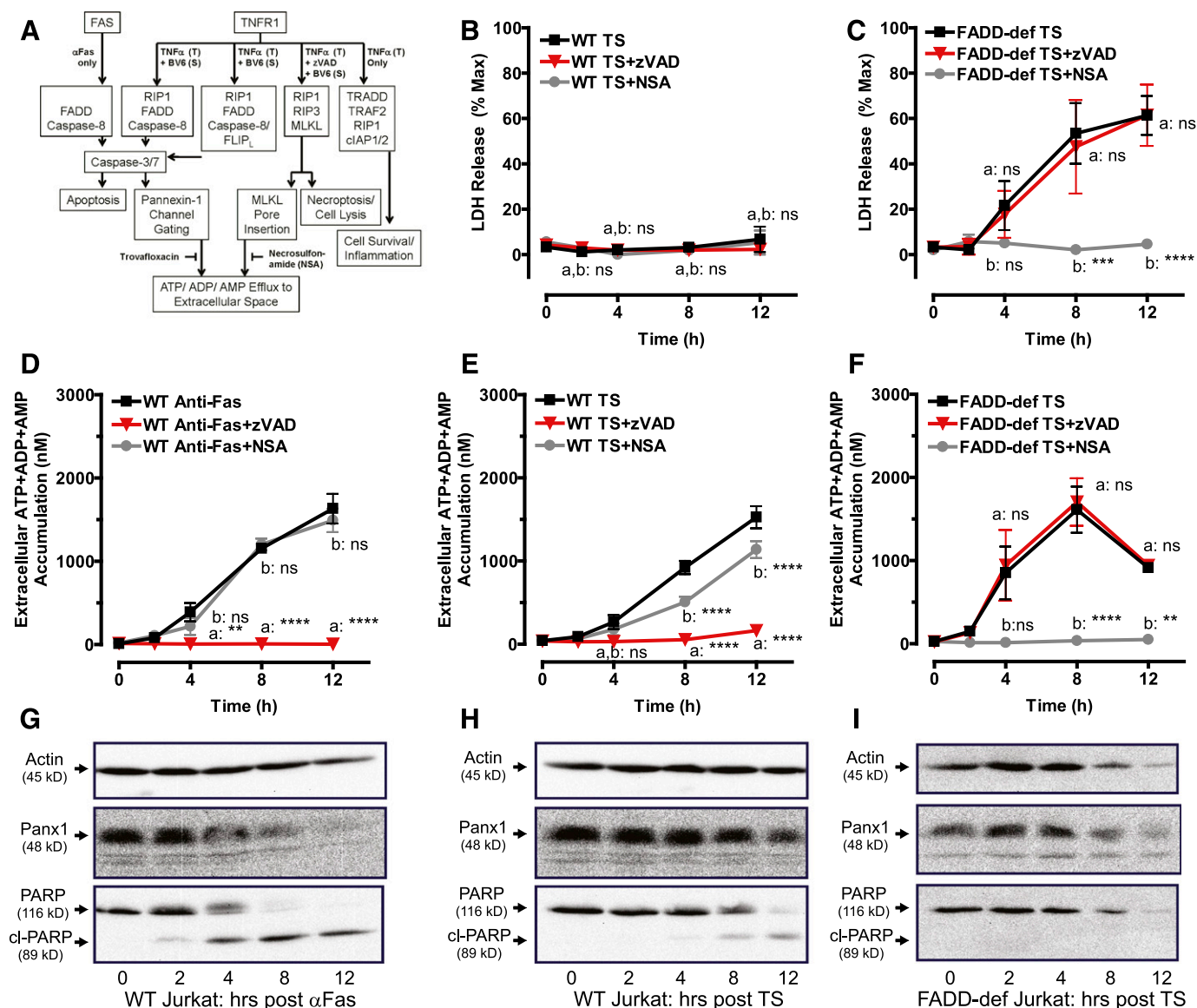


Fig. 1. TNF α -induction of necroptosis or extrinsic apoptosis induces release of adenine nucleotides from Jurkat cancer cells via mechanistically distinct pathways. (A) A schematic of cell death signaling and adenine nucleotide release pathways regulated by Fas and TNF receptors. (B, D, E) WT Jurkat cells were treated with either 250 ng/ml α Fas for the indicated times or were pretreated with 3 μ M of the Smac-mimetic BV6 for 2 hours followed by stimulation with 20 ng/ml TNF α for the indicated times. (C, F) FADD-deficient Jurkat cells were pretreated with 3 μ M BV6 for 2 hours followed by stimulation with 20 ng/ml TNF α for the indicated times. Parallel samples were stimulated with death receptor ligands in the presence or absence of 20 μ M zVAD or 1 μ M NSA as indicated. (B, C) Samples of conditioned extracellular media were collected at 0, 2, 4, 8, and 12 hours after treatment and assayed for LDH activity. LDH released from TNF α + Smac mimetic (TS)-treated cells was assayed, analyzed, and normalized to the LDH released from detergent-lysed cells. Experiments with each agent were repeated 3–4 times with data indicating mean \pm S.E. for $n = 4$ (WT) and $n = 3$ (FADD-deficient) independent experiments. Analysis by two-way analysis of variance and Tukey post-test comparison; *a*: TS-stimulated +zVAD versus -zVAD; *b*: TS-stimulated +NSA versus -NSA. (D–F) Cells were treated with either α Fas (D) or TS (E, F), and conditioned extracellular media samples were collected at 0, 2, 4, 8, and 12 hours after treatment and analyzed for summed ATP + ADP + AMP. Data indicate mean \pm S.E. of $n = 3$ independent experiments. Analysis by two-way analysis of variance and Tukey post-test comparison; *a*: α Fas- or TS-treated +zVAD versus -zVAD; *b*: TS-stimulated +NSA versus -NSA. (G–I) Whole-cell lysates were prepared at the indicated times after treatment of Western blot analysis as described in *Materials and Methods* and probed for Panx1, PARP, and actin. Data are representative of three experiments for each condition. All panels: ns, not statistically significant; ** $P < 0.01$; *** $P < 0.001$; **** $P < 0.0001$.

(APCP) was purchased from Jena Bioscience (Jena, Germany). The specificity of the noncommercial rabbit anti-human pannexin-1 (Panx1) antiserum has been described elsewhere (Penuela et al., 2007, 2009; Chekeni et al., 2010; Boyd-Tressler et al., 2014).

Cell Culture and Induction of Apoptosis and Necroptosis. WT, FADD-deficient, and RIP1-deficient Jurkat cells were maintained in RPMI-1640 medium supplemented with 10% newborn bovine calf serum (Hyclone; GE Healthcare BioSciences, Pittsburgh, PA), 100 units/ml penicillin, 100 μ g/ml streptomycin (Invitrogen, Carlsbad, CA), and 2 mM L-glutamine (Lonza, Basel, Switzerland) at

37°C in 5% CO₂. RIP1-deficient cell culture medium also contained 2.5 μ g/ml amphotericin B. For induction of apoptosis and analysis of released adenine nucleotides, the WT Jurkat cells were resuspended at 2×10^6 cells/ml (2 ml/well; 12-well plates) in RPMI-1640 as above but with 10% bovine calf serum treated for 2 hours at 65°C to inactivate serum nucleotidases. For TNF α -induced apoptosis, the resuspended cells were preincubated with 3 μ M BV6 for 2 hours at 37°C in 5% CO₂ before addition of 20 ng/ml TNF α . Apoptosis in all Jurkat cell types was induced by 3 μ M staurosporine (STS), 20 μ M etoposide (Etop), or 250 ng/ml anti-Fas.

TABLE 1
Pathways and enzymes for extracellular metabolism of nucleotides and nucleosides

Extracellular Metabolic Function	Ectoenzyme Names/Subtypes	Catalytic Reaction	Substrate Selectivity	Inhibitors (Representative)	T-Cell Expression
Ecto-ATPase, Ecto-ADPase, Apyrase	CD39 family ENTDase1-4	ATP > ADP (+Pi) > AMP (+Pi)	All purine and pyrimidine nucleotide tri/diphosphates	ARL-67156; others	Yes, but varies with differentiation and polarization state; high in Tregs
Ecto-ATP pyro-phosphatase/ phosphodiesterase	ENPP1-3	ATP > AMP (+PPi)	Purine and pyrimidine nucleotide triphosphates	β , γ -methylene-ATP (competitive substrate)	Unknown but likely
Ecto-AMPase	CD73; ecto-5'-nucleotidase; (5Nte)	AMP > Ado (+Pi)	Purine and pyrimidine nucleotide monophosphates	α , β -methylene-ADP (APCP)	Yes, but varies with differentiation and polarization state; high in Tregs
Ecto-AMPase	Tissue nonselective TNAP	AMP > Ado (+Pi)	Purine and pyrimidine nucleotide monophosphates; non-nucleotide phosphate esters	Levamisole; tetramisole	Unknown
Ecto-AMPase, Ecto-Phosphatase	TM-PAP	AMP (and ATP) > Ado (+Pi)	Purine and pyrimidine nucleotide phosphates; non-nucleotide phosphate esters	L-Tartrate; some cyclic AMP analogs	Yes, but varies with differentiation and polarization state
Ecto-AMP Deaminase	AMPD3	AMP > IMP	AMP	Pentostatin/deoxycoformycin	Unknown
Ecto-Adenosine Deaminase	Ecto-ADA	Ado > Ino	AMP	Pentostatin/deoxycoformycin	Yes
Nucleoside transport (concentrative)	CNT (multiple subtypes)	Extracellular nucleoside > intracellular nucleoside	All natural nucleosides; many nucleoside analogs	Dipyridamole; many others	Yes
Nucleoside transport (equilibrative)	ENT (multiple subtypes)	Extracellular nucleoside > intracellular nucleoside	All natural nucleosides; many nucleoside analogs	Dipyridamole; many others	Yes

AMPD, AMP deaminase; CNT, concentrative nucleoside transporter; ENT, equilibrative nucleoside transporter; Tregs, regulatory T cells.

For induction of necroptosis, FADD-deficient Jurkat cells were resuspended at 2×10^6 cells/ml and preincubated with $3 \mu\text{M}$ BV6 for 2 hours at 37°C in 5% CO_2 before addition of 20 ng/ml TNF- α . Where indicated, $20 \mu\text{M}$, $50 \mu\text{M}$, or $100 \mu\text{M}$ zVAD, $1 \mu\text{M}$ NSA, or $30 \mu\text{M}$ trovafloxacin (Trova) were added to the cell cultures 1 hour before addition of TNF- α , anti-Fas, STS, or Etop. Where indicated, $50 \mu\text{M}$ APCP was added 10 minutes before the addition of TNF- α , anti-Fas, STS, or Etop.

Collection of Conditioned Medium and Measurement of Released Adenine Nucleotides. Conditioned medium from control, apoptotic, or necroptotic Jurkat cells was collected and assayed for accumulation of extracellular adenine nucleotides as described elsewhere (Boyd-Tressler et al., 2014). Briefly, samples of the conditioned medium supernatants were taken at indicated times (routinely 0, 2, 4, 8, 12 hours) after addition of TNF- α , anti-Fas, STS, or Etop and centrifuged at 13,500 RPM for 15 seconds to pellet cells. The cell-free supernatants were transferred to fresh tubes for analysis of either ATP only or total adenine nucleotides (ATP + ADP + AMP).

For luciferase-based quantification of ATP only, a $50\text{-}\mu\text{l}$ aliquot of conditioned medium supernatant was supplemented with $46 \mu\text{l}$ of FLAAB and $4 \mu\text{l}$ of concentrated FLAAM (reconstituted with 5 ml of sterile water per vial of lyophilized luciferase/luciferin mix) and transferred to a well of a 96-well white plate. The ATP-dependent bioluminescence was measured with a BioTek Synergy HT plate reader (1 second integration of emitted light; BioTek Instruments, Winooski, VT) and quantified by comparison with ATP standards assayed under identical conditions.

For quantification of total adenine nucleotides, the samples were subjected to a protocol modified from that described in Hampp (1985) whereby AMP and ADP were rephosphorylated to ATP (in a cycling reaction driven by excess phosphoenolpyruvate in the presence of pyruvate kinase and myokinase) before the luciferase analysis described earlier. We supplemented $50 \mu\text{l}$ of conditioned medium supernatant with $8.3 \mu\text{l}$ of rephosphorylation cocktail (25 mM K-HEPES, pH 8.0, 50 mM MgSO_4 , 8.3 mM phosphoenolpyruvate, 600 U/ml myokinase, 300 U/ml pyruvate kinase) and incubated the medium for 90 minutes at 37°C . We then added $37.7 \mu\text{l}$ FLAAB and $4 \mu\text{l}$ concentrated FLAAM to each rephosphorylated sample and measured the ATP-dependent bioluminescence.

Measurement of Cell Lysis by LDH Release. Cells were treated with apoptotic or necroptotic stimuli as described earlier. After brief centrifugation of the cell suspensions, the cell-free supernatants were assayed for LDH enzyme activity using the cytotoxicity detection kit according to the protocol of Roche Applied Science. The released LDH was normalized to total LDH content measured in 1% Triton X-100-permeabilized samples of untreated Jurkat T cells.

Western Blot Analyses. We centrifuged 1-ml aliquots of 2×10^6 Jurkat cells, and the cell pellets were washed in phosphate-buffered saline (PBS). Whole-cell lysates were prepared by detergent-based extractions before standard processing by SDS-PAGE (either 12% or 4–20% polyacrylamide), transfer to polyvinylidene fluoride membranes, and Western blot analysis as described elsewhere (Boyd-Tressler et al., 2014). Primary antibodies were used at the following concentrations or dilutions: anti-human pannexin 1 (1:5000), anti-PARP (1:1000), anti- β -actin ($1 \mu\text{g/ml}$), or anti-PAP ($1 \mu\text{g/ml}$). Horseradish peroxidase-conjugated secondary antibodies were used at a final concentration of $0.13 \mu\text{g/ml}$. The chemiluminescent images of the blots were developed with electrochemiluminescence reagent, then imaged and quantified using FluorChemE processor and AlphaView SA imaging software (ProteinSimple, San Jose, CA).

YO-PRO Dye Influx. We treated $500\text{-}\mu\text{l}$ aliquots of Jurkat cell suspension (10^6 /ml) with apoptotic stimuli as described earlier for various times; then we collected pellets by centrifugation and washed them once with PBS. The washed cell pellets were resuspended in $500 \mu\text{l}$ of basal salt solution (BSS) containing 130 mM NaCl, 5 mM KCl, 1 mM MgCl_2 , 1.5 mM CaCl_2 , 25 mM Na HEPES, pH 7.5, 5 mM glucose, and 0.1% bovine serum albumin (BSA). We added $1 \mu\text{M}$ YO-PRO dye, and the cells were incubated for 20 minutes. The cells were then pelleted by brief

centrifugation, washed once in PBS, and resuspended in 500 μ l of fresh BSS. We transferred 200- μ l aliquots to wells in a 96-well plate. The fluorescence (485 nm/540 nm) was measured on the BioTek Synergy HT plate reader. Phase-contrast and epifluorescence images of the cells in each well were then recorded using a Zeiss Axiovert 25 Microscope (Carl Zeiss, Thornwood, NY) equipped with a 485 nm/540 nm filter set, QCam1394 digital camera, and QCapturePro imaging software (QImaging, Surrey, BC, Canada).

Calcein Dye Efflux. Jurkat cells were suspended at 2×10^6 cells/ml in RPMI + 10% heat-inactivated calf serum + 100 units/ml penicillin, 100 μ g/ml streptomycin, and 2 mM L-glutamine. The suspensions were supplemented with 1 μ M calcein-AM and 250 μ M probenecid and incubated for 45 minutes at 37°C. The cells were washed in PBS, resuspended in the same RPMI test medium, and then treated with 3 μ M STS in the presence or absence of 100 μ M zVAD or 30 μ M Trova for 4 hours at 37°C and 5% CO₂. After brief centrifugation, the cell pellets were washed and resuspended in BSS + 5 mM glucose + 0.1% BSA, and the fluorescence (485 nm/528 nm) was measured on the BioTek Synergy HT plate reader.

Imaging of Mitochondrial Localization. We incubated 1×10^6 Jurkat cells/ml for 4 hours with or without 3 μ M STS. The cells were pelleted, washed with PBS, and resuspended in prewarmed (37°C) staining solution consisting of 500 nM MitoTracker Red CM-H₂XRos in BSS + 5 mM glucose + 0.1% BSA and incubated for 30 minutes at 37°C in the dark. The cells were pelleted, washed in PBS, resuspended in BSS + 5 mM glucose + 0.1% BSA supplemented with a 1:100 dilution of DAPI (0.2 μ g/ml working stock), and incubated in the dark at room temperature for 5–10 minutes. The cells were pelleted, washed in PBS, fixed in 200 μ l of 4% paraformaldehyde in PBS for 15 minutes at 37°C. The fixed cells were repelleted, washed, and resuspended in 50 μ l 0.5% paraformaldehyde and stored at 4°C. Images of the cells were acquired using an Olympus FluoView FV1000 laser scanning confocal microscope coupled with an IX-81 inverted microscope equipped with a 60 \times /1.42 NA oil immersion objective and a computer running FluoView FV10-ASW version 3.1b software (Olympus America, Center Valley, PA).

Extracellular ATP and AMP Hydrolysis Assays. WT, FADD-deficient, or RIP1-deficient cells were resuspended at 2×10^6 cells/ml in the RPMI assay medium for assay of extracellular AMP hydrolysis or in BSS + 5 mM glucose + 0.1% BSA for assay of extracellular ATP hydrolysis. After addition of 1 μ M AMP or ATP, the cell suspensions were incubated for 30 minutes at 37°C, and then centrifuged at 13,500 RPM for 15 seconds to pellet the cells. The cell-free supernatants were collected and assayed for ATP or AMP by the luciferase-based methods described earlier. Where indicated, 50 μ M APCP, 5 mM tetramisole, 200 μ M pentostatin, or 100 μ M ARL-67156 was added to the cell suspension 10 minutes before the addition of AMP or ATP.

High-Pressure Liquid Chromatography Assays of Extracellular AMP Metabolism and Adenosine/Inosine Accumulation or Extracellular Etheno-AMP Metabolism and Etheno-Adenosine Accumulation. Wild-type, FADD-deficient, or RIP1-deficient cells were suspended at 2×10^6 cells/ml in BSS + 5 mM glucose + 0.1% BSA and preincubated for 15 minutes at 37°C. The cell suspensions were supplemented with 10 μ M 1,N6-etheno-AMP (ϵ -AMP) or 100 μ M AMP plus or minus various inhibitors, as indicated, then incubated for 30 minutes at 37°C and centrifuged at 13,500 RPM for 15 seconds. The cell-free supernatants were transferred to new tubes, boiled for 5 minutes at 100°C, then placed on ice. Extracellular ϵ -AMP and etheno-adenosine (ϵ -ADO) were resolved by and quantified by ion exchange HPLC using a Bio-Rad Gradient Module high-pressure liquid chromatography (HPLC) connected to a Linear Fluor LC305 fluorescence detector (Bio-Rad Laboratories, Hercules, CA). Samples were diluted 1:10 in water, and 50 μ l was injected onto a Hamilton PRP-X100 anion exchange column (Hamilton Robotics, Reno, NV), which was eluted at 1.0 or 1.6 ml/min with a gradient of NH₄HCO₃ in 30% methanol. The baseline mobile phase was 0.25 M NH₄HCO₃ (pH 8.5) in 30% methanol.

After sample injection, the mobile phase was developed linearly from 0.25 to 0.275 M NH₄HCO₃ for 8 minutes, remained isocratic at

0.275 M NH₄HCO₃ for the next 4 minutes, was washed for 3 minutes at 0.425 M NH₄HCO₃, and then was re-equilibrated back to the baseline mobile phase for 15 minutes. Extracellular AMP, IMP, adenosine, and inosine were resolved by reverse HPLC using the Bio-Rad Gradient Module HPLC connected to an absorbance detector. Samples were diluted 1:10 in water, and 50 μ l was injected onto a Alltech C18 Nucleotide/Nucleoside reverse phase column (Alltech, Woodridge, IL), which was eluted at 1.0 ml/min with a gradient of methanol in 20 mM (NH₄)₃HPO₄ (pH 6.0). The baseline mobile phase was 20 mM (NH₄)₃HPO₄ (pH 6.0) in 0% methanol.

After sample injection, the column was eluted with isocratic 0% methanol for 4 minutes followed by an gradient increase to 8% methanol from 4 to 6 minutes, a gradient increase to 20% methanol from 6 to 8 minutes, isocratic elution with 20% methanol from 8 to 18 minutes, a gradient decrease to 0% methanol from 18 to 20 minutes, and then isocratic elution with 0% methanol to re-equilibrate the column to the baseline condition. Absorbance of eluate was continuously recorded at 260 nm. Injection with standard solutions of 100 μ M IMP, AMP, inosine, or adenosine were used to identify the retention time of those nucleotides and nucleosides. Chromatogram peaks were obtained with Data Ally v2.06 software (LabAlliance, Scientific Systems, Inc., State College, PA).

Assay of Ecto-Nitrophenyl Phosphatase Activity in Jurkat Cells. We plated 200- μ l aliquots of WT, RIP1-deficient, and FADD-deficient Jurkat cells (2×10^6 /ml) in 96-well plates. The cells were suspended in BSS (+ glucose + BSA) that was buffered to pH 7.5 or pH 6.5. The cell suspensions were supplemented with 500 μ M *p*-nitrophenyl phosphate in the absence or presence of 10 mM L-tartrate (sodium salt) or 50 μ M APCP, and they were incubated for 18 hours at 25°C. Hydrolysis of nitrophenyl phosphate to nitrophenyl was assayed by measuring absorbance at 405 nm on the BioTek Synergy HT plate reader.

Quantitative RT-PCR Analysis of CD73 Expression. Total RNA was extracted by TRIzol reagent from WT, FADD-deficient, or RIP1-deficient Jurkat cells by standard methods. The All-in-One First-Strand cDNA Synthesis kit (GeneCopoeia, Rockville, MD) was used for synthesis of first-strand cDNA from purified RNA. Quantitative RT-PCR analysis of CD73 or GAPDH mRNA was performed using a StepOne-Plus Real-Time PCR System (Applied Biosystems, Foster City, CA). The reactions were performed in 20- μ l reaction volumes containing All-in-One qPCR Mix with ROX reference dye, 0.2 μ M PCR primers, and 1:100 dilution of the first strand cDNA reaction, and they were run in triplicate. The relative expression was calculated using the $\Delta\Delta C_t$ method using StepOne software v. 2.1 (Applied Biosystems) with values normalized to the reference gene GAPDH; the relative differences in CD73 mRNA levels in FADD-deficient or RIP1-deficient cells were normalized to the values in measured in WT Jurkat cells.

Data Analysis. Experiments were repeated 3–6 times with separate Jurkat cell culture preparations. Western blot results are from representative experiments. Figures illustrating quantification of extracellular adenine nucleotide accumulation, LDH release, extracellular nucleotide hydrolysis, YO-PRO dye influx, and calcein dye efflux represent the mean (\pm S.E.) of data from three to six independent experiments each performed with two to four technical replicates. Quantitative results were analyzed by *t*-test or two-way analysis of variance with Tukey post-test comparison using Prism 6.0 software (GraphPad Software, San Diego, CA).

Results

TNF α -Induction of Necroptosis or Extrinsic Apoptosis Induces Release of Adenine Nucleotides from Jurkat Cells via Mechanistically Distinct Pathways. T-cell leukemias or lymphomas have been widely used as tumor cell models for examining the relationships between Panx1-mediated ATP release, extracellular ATP/AMP metabolism, adenosine accumulation, and the modulation of anti-tumor immune responses in vivo and in vitro (Elliott et al., 2009; Ghiringhelli et al., 2009;

Martins et al., 2009; Chekeni et al., 2010; Poon et al., 2014). We previously described roles for Panx1 channels in the release of both ATP and AMP during chemotherapeutic drug-induced apoptosis of Jurkat human leukemic T cells (Boyd-Tressler et al., 2014). In WT Jurkat human leukemic T cells, TNF- α (T) binding to type 1 TNF receptors (TNFR1) induces formation of complex 1 signaling platforms. However, when these cells are treated with Smac mimetic drugs such as BV6, the cIAPs are down-regulated to facilitate the assembly of complex 2. Under these conditions, caspase-8 is activated to both initiate apoptosis and inactivate RIP1. Conversely, when Jurkat cells deficient in FADD (FADD-deficient) are treated with TNF- α plus BV6, complex 2 cannot assemble, leaving RIP1 free to form necrosome platforms that license RIP3-dependent MLKL pore formation and necroptosis.

Fas receptor-induced apoptosis of WT Jurkat cells has been previously shown to elicit ATP efflux via caspase-3-mediated cleavage of the C terminus of Panx1 channels (Fig. 1A). The kinetics and magnitude of this Fas-induced ATP release from Jurkat cells have been defined (Chekeni et al., 2010), but it is not known whether similar Panx1 cleavage and ATP efflux parameters characterize TNFR1-induced apoptosis or how MLKL pores may facilitate alternative ATP efflux parameters during TNFR1-induced necroptosis.

Using WT and FADD-deficient Jurkat cells identically cotreated with TNF- α plus BV6 Smac mimetic, we compared the kinetics of lytic plasma membrane disruption (as indicated by release of the cytosolic macromolecule LDH) during apoptotic versus necroptotic progression. The WT cells treated with TNF- α plus BV6 for up to 12 hours did not release LDH (Fig. 1B), but FADD-deficient cells began to release LDH within 4 hours, and this progressively increased to ~60% cell lysis by 12 hours (Fig. 1C). The TNF- α plus BV6-induced lysis of FADD-deficient cells was completely suppressed by NSA, an inhibitor of the phosphorylated MLKL oligomerization necessary for insertion of MLKL pores into the plasma membrane (Sun et al., 2012). In contrast, there was no attenuation of LDH release from FADD-deficient cells treated with TNF- α plus BV6 in the presence of the pan-caspase inhibitor zVAD (Fig. 1C). These observations confirm that TNF- α -induced necroptotic signaling is defined by rapid plasma membrane disruption independently of apoptotic caspases and that TNF- α induced apoptotic signaling over a similar 12-hour test period does not result in secondary necrosis.

Despite these marked differences in lytic plasma membrane disruption, TNF- α plus BV6 induced similar extracellular adenine nucleotide accumulation (1–1.5 μ M at 8–12 hours) by the WT and FADD-deficient Jurkat cells cultured at 2×10^6 /ml. We characterized the kinetics and underlying apoptotic mechanism of TNF- α plus BV6-induced adenine nucleotide release from the WT cells by using Fas receptor activation as a positive control and measuring the summed accumulation of extracellular ATP, ADP, and AMP (ATP + ADP + AMP).

Our previous study (Boyd-Tressler et al., 2014) determined that analysis of ATP + ADP + AMP, rather than ATP alone, provides a better readout of net Panx1 channel-mediated adenine nucleotide efflux during apoptotic progression because the intracellular nucleotide pool shifts from initially high [ATP] and low [ADP] + [AMP] to lower [ATP] and higher [ADP] + [AMP] as a consequence of the increased ATP utilization and decreased mitochondrial ATP synthesis that characterizes apoptotic signaling (Ricci et al., 2004; Waterhouse et al., 2001). TNF- α plus BV6-induced apoptosis resulted in a

steady and significant increase in ATP + ADP + AMP after a ~4-hour lag time, and this was suppressed in the presence of zVAD but not NSA (Fig. 1E). These ATP + ADP + AMP accumulation responses were similar to those observed in α Fas-treated WT Jurkat cells but with modestly slower kinetics (Fig. 1D). In both TNF- α plus BV6-treated and α Fas-treated WT Jurkat cells, the time course of the ATP + ADP + AMP accumulation correlated with the activation of caspase-3 as indicated by cleavage of the canonical substrate PARP (Fig. 1, G and H).

We also compared the proteolytic processing of Panx1 channels during the TNF- α plus BV6 treatment versus α Fas treatment. Panx1 exists in three different glycosylation states: unglycosylated Gly-0, monoglycosylated Gly-1, and Gly-2, which is the fully glycosylated and most abundant form that accumulates in the plasma membrane as a 48–50 kDa protein (Penuela et al., 2007, 2013). All three forms are detected using a previously characterized polyclonal antibody that recognizes the extreme intracellular C terminus of Panx1 downstream of the caspase-3 cleavage site (Chekeni et al., 2010; Boyd-Tressler et al., 2014). Caspase-3-mediated cleavage of Panx1 during apoptotic progression results in a decreased anti-Panx1 48–50 kDa band on Western blots of whole-cell lysates due to loss of the antibody-binding site. Panx1 cleavage was evident within 4 hours in α Fas-treated WT cells and within 8 hours in the TNF- α plus BV6-treated cells (Fig. 1, G and H).

These data, together with the observed lack of LDH release, indicate that the ATP + ADP + AMP accumulation triggered during TNF-receptor mediated apoptosis is mediated by efflux through caspase-3-activated Panx1 channels before secondary necrosis. This confirms that engagement of multiple death receptors in Jurkat leukemia cells activates similar extrinsic apoptotic signaling programs, leading to proteolytic gating of Panx1 channels that mediate efflux of cytosolic ATP, ADP, and AMP pools.

In contrast to the WT cells, FADD-deficient Jurkat cells responded to TNF- α plus BV6 with robust ATP + ADP + AMP accumulation that started at 2 hours and peaked at 8 hours. This response was completely suppressed by NSA but insensitive to zVAD (Fig. 1F), indicating that extracellular adenine nucleotide accumulation was dependent on insertion of nonselective MLKL pores into the plasma membrane. Also consistent with this mechanism, no obvious cleavage of PARP or Panx1 was evident in TNF- α plus BV6-stimulated FADD-deficient Jurkat cells at the 4- and 8-hour time points, coinciding with significant nucleotide release (Fig. 1I). It is important to note that the decrease in the Panx1 (and uncleaved PARP1) Western blot signals occurring after 8 hours is due to loss of viable cell mass, as indicated by the decreased actin signal.

Taken together, these data from FADD-deficient Jurkat cells indicate that although TNFR1 signaling is redirected from extrinsic apoptosis to necroptosis, this regulated cell death results in extracellular accumulation of ATP, ADP, and AMP released via MLKL pores concurrent with cell lysis.

Intrinsic Apoptotic Signaling and Panx1 Channel Cleavage in FADD-Deficient Jurkat Cells Are Uncoupled from Accumulation of Extracellular Adenine Nucleotides. Although FADD is a critical mediator of extrinsic apoptosis by Fas or TNFR1, the assembly of RIP1/FADD/caspase-8 ripoptosomes also amplifies intrinsic apoptosis triggered by chemotherapeutic drugs due to release of mitochondrial Smac and down-regulation of IAPs (Feoktistova et al., 2011; Belz et al., 2014). We tested whether the absence of

FADD modulated Panx1-mediated accumulation of extracellular adenine nucleotides in Jurkat cells stimulated with chemotherapeutic drugs. We previously reported that multiple chemotherapeutic or proapoptotic drugs, including STS and Etop, trigger caspase-3-mediated activation of Panx1 channels and consequent adenine nucleotide efflux in WT Jurkat T cells (Boyd-Tressler et al., 2014). Using these responses in WT cells as positive controls, we similarly treated FADD-deficient Jurkat cells with STS or Etop for up to 12 hours and assayed Panx1 and PARP cleavage (Fig. 2, A and B), secondary necrosis (Fig. 2, C and D), and ATP + ADP + AMP accumulation (Fig. 2, E and F).

Both STS and Etop induced robust intrinsic apoptosis in the FADD-deficient cells as indicated by cleavage of PARP and Panx1 with similar kinetics compared with the responses in

WT cells. We verified that the FADD-deficient Jurkat cells were unable to undergo extrinsic apoptosis as indicated by the absence of PARP and Panx1 cleavage in response to α Fas (Fig. 2B). STS induced near-maximal apoptotic activation within 4 to 6 hours in both Jurkat lines whereas significant responses to Etop required 6 to 8 hours of exposure. Secondary necrosis was observed when either cell line was treated with STS (Fig. 2, C-i and D-i), but not Etop (Fig. 2, C-ii and D-ii), for >8 hours; this lytic release of LDH was completely suppressed by zVAD.

Consistent with our previous findings (Boyd-Tressler et al., 2014), STS (Fig. 2E-i) and Etop (Fig. 2E-ii) induced robust ATP + ADP + AMP accumulation in WT Jurkat cells that was: 1) temporally correlated with the kinetics of Panx1 proteolytic processing (Fig. 2A); 2) insensitive to NSA; and 3) markedly suppressed by zVAD.

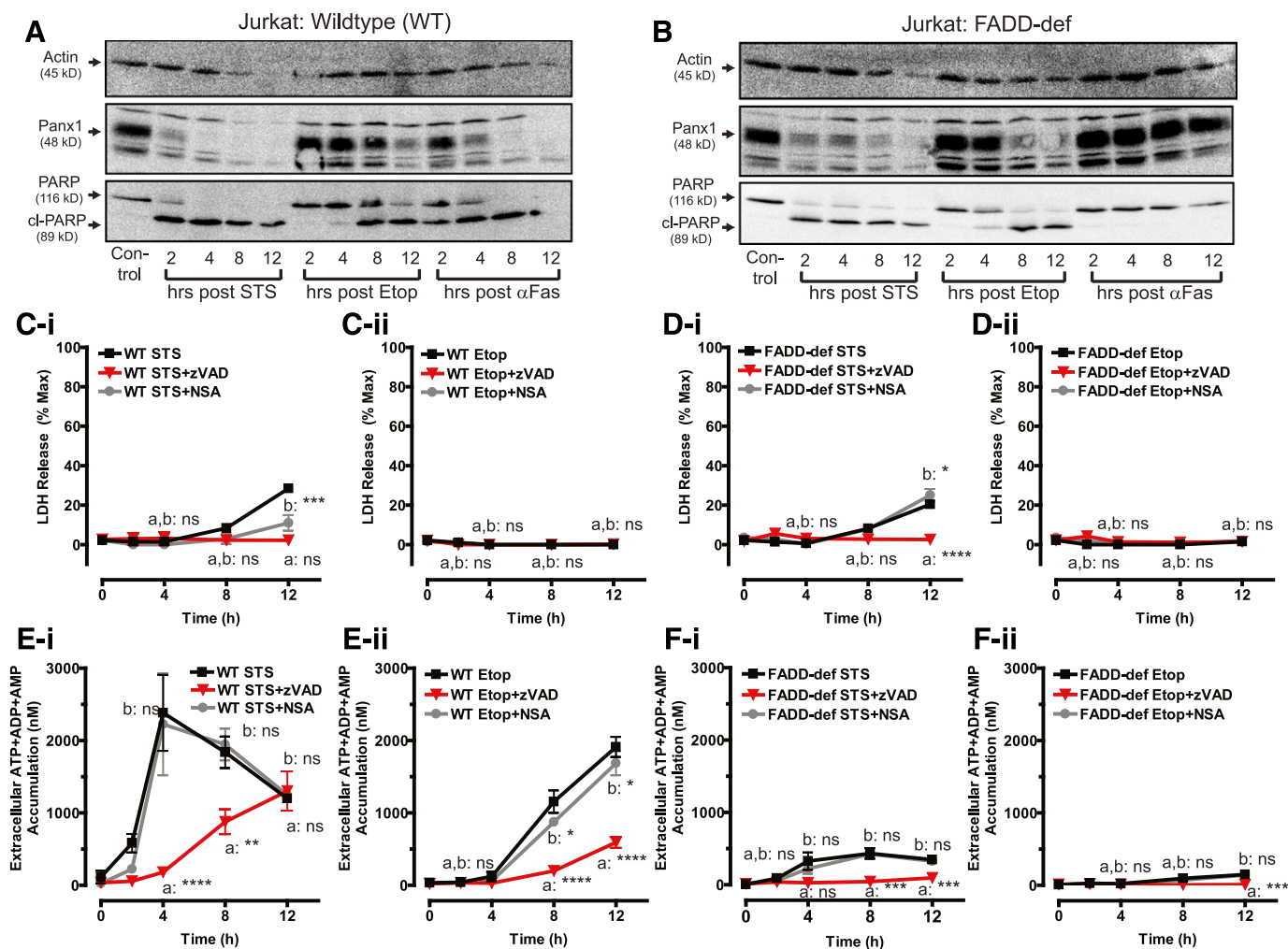


Fig. 2. Intrinsic apoptotic signaling and Panx1 channel cleavage in FADD-deficient Jurkat cancer cells is uncoupled from accumulation of extracellular adenine nucleotides. WT and FADD-deficient cells were treated with 3 μ M STS, 20 μ M Etop, or 250 ng/ml α Fas in the presence of 100 μ M zVAD or 1 μ M NSA as indicated. (A, B) Whole-cell lysates were prepared at the indicated times after treatment of Western blot analysis and probed for Panx1, PARP, and actin. Data are representative of three experiments for each cell type and condition. (C, D) Conditioned extracellular media samples were collected from STS-treated WT cells (C-i), Etop-treated WT cells (C-ii), STS-treated FADD-deficient (FADD-def) cells (D-i), or Etop-treated FADD-def cells (D-ii) at 0, 2, 4, 8, and 12 hours after treatment and assayed for release of LDH as described in Fig 1. Data indicate mean \pm S.E. of three independent experiments. Analysis by two-way analysis of variance and Tukey post-test comparison; a: STS-stimulated or Etop-stimulated +zVAD versus -zVAD; b: STS- or Etop-stimulated +NSA versus -NSA. (E, F) WT and FADD-def cells were treated with 3 μ M STS or 20 μ M Etop in the presence or absence of 100 μ M zVAD or 1 μ M NSA where indicated. Conditioned extracellular media samples were collected from STS-treated WT cells (E-i), Etop-treated WT cells (E-ii), STS-treated (FADD-def) cells (F-i), or Etop-treated FADD-def cells (F-ii) at 0, 2, 4, 8, and 12 hours after treatment and assayed for total ATP + ADP + AMP as described in *Materials and Methods*. Data indicate mean \pm S.E. of three independent experiments. Analysis by two-way analysis of variance and Tukey post-test comparison; a: STS- or Etop-stimulated +zVAD versus -zVAD; b: STS- or Etop-stimulated +NSA versus -NSA. All panels: ns, not statistically significant; * P < 0.05; ** P < 0.01; *** P < 0.001; **** P < 0.0001.

We previously demonstrated that the zVAD-insensitive component of nucleotide release in STS-treated Jurkat cells is insensitive to blockade of Panx1 channels but suppressed by intracellular Ca^{2+} buffering (Boyd-Tressler et al., 2014). To our surprise, very little extracellular ATP + ADP + AMP accumulation was observed in the FADD-deficient Jurkat cells treated with STS (Fig. 2F-i) or Etop (Fig. 2F-ii) despite the robust proteolytic processing of Panx1 channels. These data indicate that FADD deficiency uncouples accumulation of extracellular adenine nucleotides from caspase-3-mediated cleavage and activation of Panx1 channels.

Caspase-3-Cleaved Panx1 Channels Are Functionally Active in FADD-Deficient Jurkat Cells during Intrinsic Apoptosis. The decreased extracellular accumulation of ATP + ADP + AMP by apoptotic FADD-deficient Jurkat cells

might reflect: 1) lack of functional Panx1 channels; 2) altered ion selectivity or rectification properties of active Panx1 channels; 3) altered localization of ATP-producing mitochondria within the local membrane environment of active Panx1 channels; or 4) increased ecto-nucleotidase activity. As illustrated in Fig. 3A, caspase-3-mediated excision of the C-terminal autoinhibitory domains of Panx1 channels gates their permeability as ATP efflux conduits but also as influx/efflux pathways for normally impermeant organic dyes. To test whether caspase-3-processed Panx1 channels are functionally blocked in apoptotic FADD-deficient Jurkat cells, we adapted our assay previously described elsewhere (Boyd-Tressler et al., 2014) for the influx of YO-PRO²⁺, a 375-Da divalent cationic dye that intercalates with DNA to produce green fluorescence.

WT or FADD-deficient cells (control and apoptotic) were pulsed with extracellular YO-PRO²⁺ at times corresponding

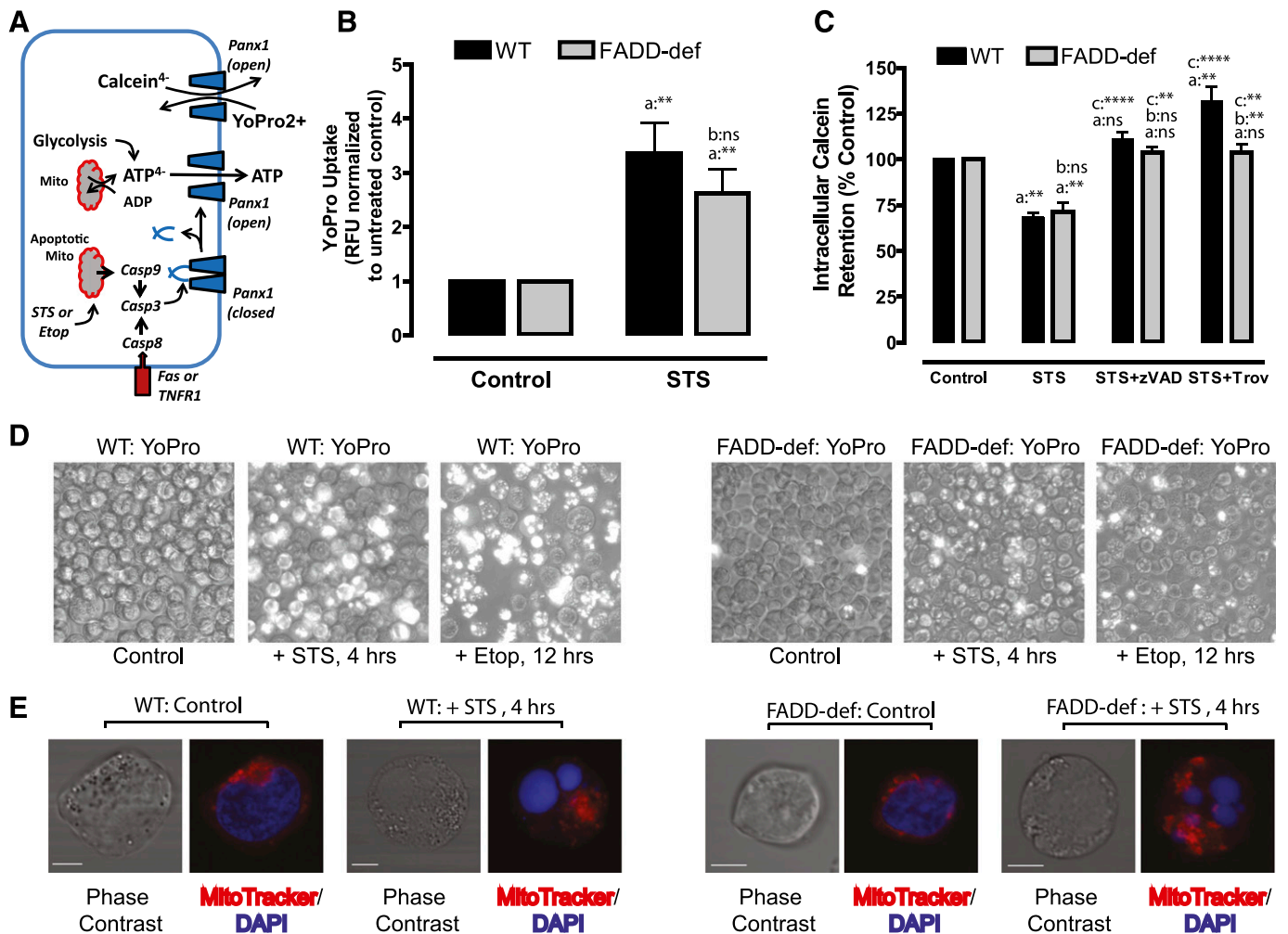


Fig. 3. Caspase-3-cleaved Panx1 channels are functionally active in FADD-deficient Jurkat cancer cells during intrinsic apoptosis. (A) Schematic illustrates caspase-3-mediated proteolytic activation of Panx1 channel function as a pathway for ATP release or efflux/influx of charged organic dyes. (B, D) WT or FADD-deficient Jurkat cells were treated with 3 μM STS for 4 hours or 20 μM Etop for 12 hours. The cells were then washed, resuspended in BSS supplemented with 1 μM YO-PRO²⁺, and incubated for 20 minutes before quantification of YO-PRO²⁺ fluorescence per well or phase-contrast/epifluorescence imaging. (B) Data indicate mean \pm S.E. from three independent experiments. Analysis by two-way analysis of variance and Tukey post-test comparison; a: +STS versus -STS; b: FADD-def versus WT. (D) Images are representative of two to three independent experiments with each stimulus. (C) WT or FADD-deficient Jurkat cells were loaded with 1 μM calcein-AM and then treated with STS for 4 hours in the presence or absence of 100 μM zVAD or 50 μM Trova. Cells were then washed and resuspended in BSS, and the calcein fluorescence was quantified. Data indicate mean \pm S.E. from three independent experiments. Analysis by two-way analysis of variance and Tukey post-test comparison; a: +STS versus -STS; b: FADD-def versus WT; c: +STS with zVAD or Trova versus +STS alone. (E) WT or FADD-deficient Jurkat cells were treated with STS for 4 hours and then stained with MitoTracker Red and DAPI. Cells were imaged by confocal microscopy at original magnification 60 \times . Data are representative images of $n = 15$ –19 individual cells. All panels: ns, not statistically significant; * $P < 0.05$; ** $P < 0.01$; *** $P < 0.001$; **** $P < 0.0001$.

to maximal Panx1 cleavage by STS (4 hours) or Etop (12 hours), and dye uptake was quantified by fluorescence plate reader analysis (Fig. 3B) and visualized by fluorescence microscopy (Fig. 3D). Significant increases in YO-PRO²⁺ dye uptake were observed in both WT and FADD-deficient cells treated with STS relative to untreated controls for each cell line (Fig. 3B). Although the quantified magnitude of YO-PRO²⁺ accumulation was modestly lower in the apoptotic FADD-def cells relative to apoptotic WT cells, these data indicate that intrinsic apoptosis does induce accumulation of functionally active Panx1 channels in the FADD-deficient Jurkat cells.

However, this assay of Panx1 function measures the influx of an organic cation whereas ATP/AMP are organic anions that efflux from the cell. To test whether FADD deficiency might alter the ion selectivity or rectification properties of Panx1 channels, we loaded WT or FADD-deficient Jurkat cells with the anionic calcein⁴⁻ dye before the 4-hour treatment with STS. Similar amounts of calcein⁴⁻ were released from the apoptotic WT and FADD-deficient cells (Fig. 3C). We confirmed that this calcein⁴⁻ efflux was mediated by caspase-3-activated Panx1 channels by performing parallel measurements in the presence of zVAD or the Panx1 channel blocker Trova (Poon et al., 2014). Both inhibitors caused complete retention of calcein⁴⁻ within the WT and FADD-deficient cells during STS treatment. These results indicate that changes in Panx1 channel ion selectivity, conductance, or rectification are unlikely mechanisms for the marked suppression of extracellular adenine nucleotide accumulation in FADD-deficient Jurkat cells.

FADD Deficiency Does Not Alter Mitochondrial Localization in Control or Apoptotic Jurkat Cells. Recent studies have reported that during T-cell activation mitochondria translocate to the plasma membrane subdomains of the immune synapse, resulting in highly localized increases in ATP concentration near to Panx1 channels and T-cell receptor signaling complexes (Quintana et al., 2007; Junker and Hoth, 2011). Ledderose et al. (2014) demonstrated that these local pools of ATP are necessary for optimal ATP release via Panx1 channels in T cells and that inhibition of mitochondrial translocation results in decreased ATP efflux. Given the T-cell lineage of the Jurkat leukemia cells, we considered the possibility that mitochondria might also localize at the plasma membrane during apoptosis to support Panx1-mediated ATP efflux and that FADD deficiency might disrupt this localization to decrease release of adenine nucleotides.

We used MitoTracker Red to visualize mitochondrial localization in WT and FADD-deficient Jurkat cells before and after STS treatment of 4 hours (Fig. 3E). DAPI staining verified that the nucleus occupies much of the cytoplasmic volume in both cell lines before apoptotic induction and that mitochondria are localized to the thin shell of cytosol between the nucleus and plasma membrane. STS induced equivalent nuclear fragmentation in the WT and FADD-deficient cells, resulting in similar diffusion of mitochondria into the expanded cytosolic volume. These data neither rule out nor demonstrate a role for subcellular mitochondrial localization in supporting Panx1-mediated ATP efflux from apoptotic Jurkat cells, but there is no indication that FADD deficiency significantly alters mitochondrial distribution.

CD73 Ecto-5'-Nucleotidase Is Up-regulated in FADD-Deficient Jurkat Cells to Rapidly Metabolize AMP Released during Apoptosis or Necroptosis. We next tested whether the decreased ATP + ADP + AMP accumulation by apoptotic FADD-deficient Jurkat cells was due to increased extracellular breakdown of adenine nucleotides released via active Panx1 channels. The most widely studied ectonucleotidases (Table 1) are the CD39-family proteins, which break down ATP and ADP to AMP, and CD73, which hydrolyzes AMP to adenosine (Resta et al., 1998; Picher et al., 2003; Robson et al., 2006; Yegutkin, 2008; Stagg and Smyth, 2010). Although both CD39 and CD73 can be up-regulated in certain types of cancers, CD73 in particular has been linked to chemotherapy-resistant cancers, and high CD73 levels are an indicator of poor prognosis (Dzhandzhugazyan et al., 1998; Stagg and Smyth, 2010; Stagg et al., 2011; Antonioli et al., 2013b; Loi et al., 2013; Young et al., 2014; Nevedomskaya et al., 2016).

As noted previously, we routinely measured the summed accumulation of extracellular ATP, ADP, and AMP by apoptotic cells because the progressive decline in the intracellular ATP/AMP ratio results in greatly increased efflux of AMP, rather than ATP, via activated Panx1 channels as the cells transition from early to later phases of the apoptotic cascade. Indeed, comparison of the magnitudes of the summed extracellular [ATP + ADP + AMP] (Fig. 4A-i; replotted data from Fig. 2, E-i and F-i) versus [ATP] alone (Fig. 4A-ii) during STS treatment of WT Jurkat cells demonstrates ATP constitutes only a minor percentage of the total adenine nucleotide release. However, a similar accumulation of extracellular ATP was observed during the first 4 hours of STS in both WT and FADD-deficient cells, which contrasted with the ~10-fold difference in extracellular [ATP + ADP + AMP] at these time points. These data suggest that Panx1-mediated ATP and AMP efflux are similar in both cell lines but that the AMP is rapidly cleared from the extracellular compartment.

Similar comparisons of ATP + ADP + AMP (Fig. 4B-i) versus ATP (Fig. 4B-ii) accumulation in WT and FADD-deficient cells during the slower apoptotic progression induced by Etop revealed a different pattern of extracellular nucleotide dynamics. Etop induced similar time courses of ATP and ATP + ADP + AMP accumulation in the WT cells (near-linear increases with time after an initial 4-hour lag period), but almost no accumulation above basal levels of either ATP or ATP + ADP + AMP in the FADD-deficient cells. This suggests both ATP and AMP can be efficiently cleared from the extracellular compartment of the FADD-deficient cells due to the slower rates of Panx1-mediated ATP and AMP efflux triggered by Etop-induced versus STS-induced apoptotic execution.

T cells can dynamically up-regulate or down-regulate expression of various ectonucleotidases, including CD73, depending on their differentiation, polarization, or activation state (Deaglio et al., 2007; Antonioli et al., 2013b; Bono et al., 2015). Previous studies have shown that WT Jurkat T cells express very low CD39 and CD73 activity (Yegutkin et al., 2002) but that multidrug resistant clonal variants of Jurkat cells, selected for suppressed Fas expression, have increased CD73 expression (Mikhailov et al., 2008). Given that: 1) AMP is the predominant nucleotide released via Panx1 channels in apoptotic Jurkat cells (and other cell types; Yamaguchi et al., 2014), and 2) CD73 can be dynamically up-regulated or

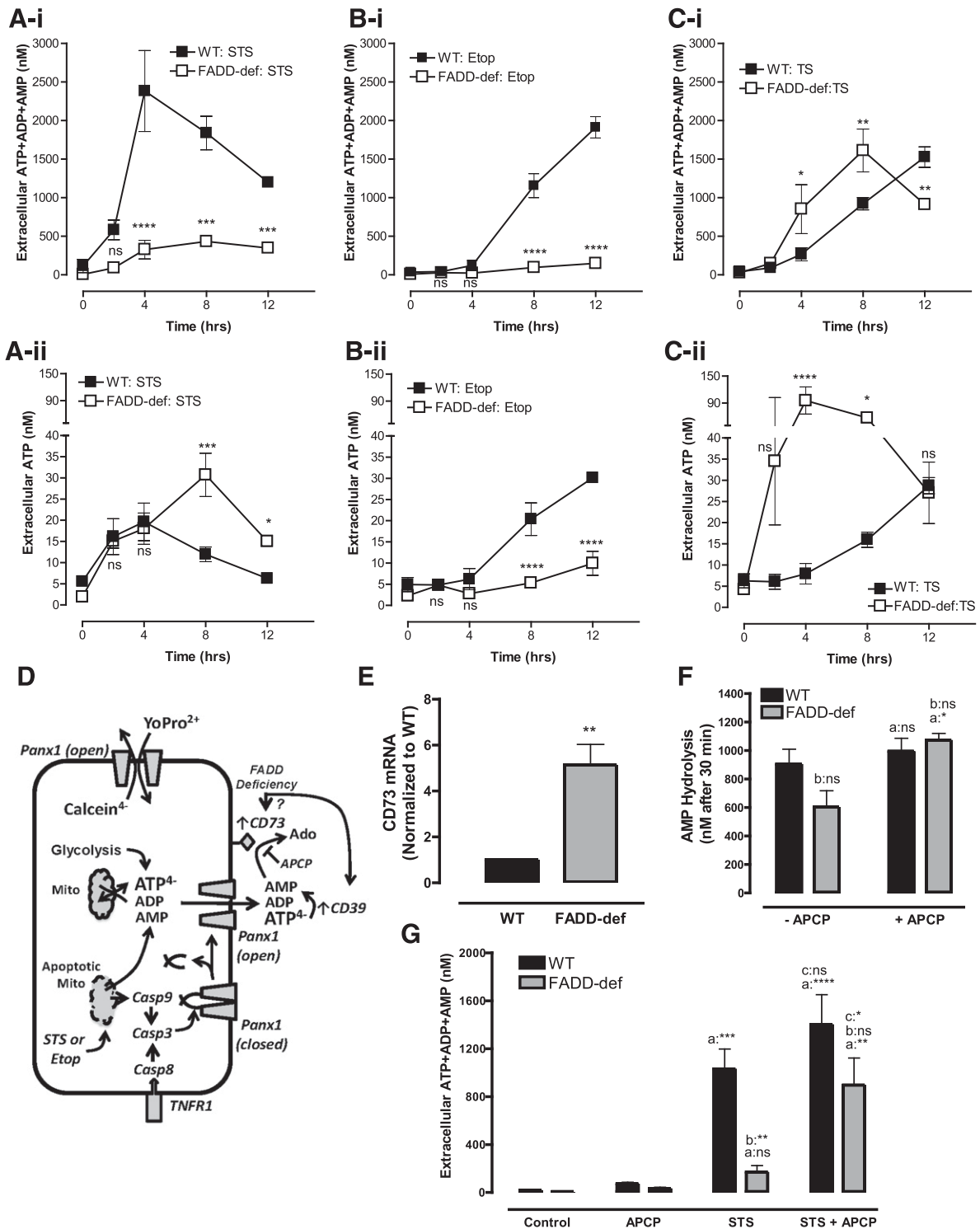


Fig. 4. CD73 ecto-5'-nucleotidase is up-regulated in FADD-deficient Jurkat cells to rapidly metabolize AMP released during apoptosis or necroptosis. (A–C) WT and FADD-deficient cells were treated with 3 μ M STS (A-i and A-ii), 20 μ M Etop (B-i and B-ii), or TNF α plus BV6 Smac-mimetic (TS) (C-i and C-ii). Conditioned medium samples were collected at 0, 2, 4, 8, and 12 hours and assayed for either summed ATP + ADP + AMP (A-i; B-i, C-i) or ATP only (A-ii, B-ii, C-ii). Data indicate mean \pm S.E. of three experiments and statistical analyses (two-way analysis of variance with Tukey post-test comparison) of the values of FADD-def versus WT at each time point. (D) Schematic of interactions between Panx1 channel-mediated adenosine nucleotide efflux and metabolism of the released nucleotides by CD39 and CD73 ectonucleotidases (APCP) during extrinsic or intrinsic apoptosis. (E) qRT-PCR analysis of CD73 mRNA expression in WT and FADD-deficient cells. Signals in FADD-def were normalized to signals in WT and represent values from three independent experiments; analysis by two-tailed *t* test. (F) We added 1 μ M exogenous AMP to suspensions (2×10^6 /ml) of untreated WT or FADD-deficient Jurkat cells in the presence or absence of 50 μ M APCP. Cell-free supernatants were collected after 30 minutes and analyzed for the concentration of remaining [AMP]. Data indicate mean \pm S.E. of four independent experiments with WT cells and three independent experiments with FADD-def cells. Analysis by two-way analysis of variance and Tukey post-test comparison; *a*: +APCP versus –APCP; *b*: FADD-def versus WT. (G) WT or FADD-deficient Jurkat cells were treated with 3 μ M STS for 4 hours in the absence or presence of 50 μ M APCP. Conditioned medium samples were collected and assayed for summed ATP + ADP + AMP. Data indicate mean \pm S.E. of six independent experiments with

down-regulated during polarization and activation of normal T lymphocytes, we hypothesized that FADD-deficiency resulted in an increased CD73 activity to efficiently hydrolyze released AMP to adenosine (Fig. 4C).

Comparative qRT-PCR analysis revealed that CD73 mRNA levels were ~5-fold greater in the FADD-deficient cells relative to WT Jurkat cells (Fig. 4E). We compared the abilities of FADD-deficient versus WT Jurkat cells to hydrolyze a 1 μ M pulse of exogenous AMP over a 30-minute test period in the absence or presence of APCP. The latter is a well-characterized inhibitor of CD73 activity (Resta et al., 1998; Bhattarai et al., 2015). The WT cells hydrolyzed less than 15% of the added AMP in 30 minutes while the FADD-deficient cells cleared 40% of the AMP, and this accelerated breakdown was suppressed by APCP (Fig. 4F).

We then compared the magnitudes of ATP + ADP + AMP accumulation by WT and FADD-deficient Jurkat cells during 4 hours of STS treatment in the absence or presence of APCP. The presence of 50 μ M APCP markedly increased (by 5-fold) ATP + ADP + AMP accumulation in the STS-stimulated FADD-deficient cells; this level of extracellular summed adenine nucleotide was similar to that in STS-treated WT cells in the absence of APCP (Fig. 4G). Similar potentiation of extracellular adenine nucleotide accumulation by APCP was observed in FADD-deficient cells treated with Etop for 12 hours (data not shown). The ability of APCP to increase [ATP + ADP + AMP] was not observed when the FADD-deficient cells were cotreated with STS and zVAD (not shown); this is consistent with AMP being released via caspase-3-gated Panx1 channels.

Comparison of ATP + ADP + AMP (Fig. 4C-i) versus ATP (Fig. 4C-ii) accumulation during TNF α plus BV6-induced apoptosis in WT cells versus TNF α plus BV6-induced necroptosis in FADD-deficient cells yielded additional extracellular nucleotide kinetic profiles. The kinetics and magnitudes of ATP + ADP + AMP accumulation during TNF α plus BV6-induced extrinsic apoptosis (Fig. 4C-i) in WT cells were very similar (4-hour lag phase followed by steady increase over the next 8 hours) to those measured during Etop-induced intrinsic apoptosis of WT cells (Fig. 4B-i). Likewise, the kinetics of ATP release from apoptotic WT cells in response to TNF α plus BV6 (Fig. 4C-ii) or Etop (Fig. 4B-ii) were similar. In contrast, necroptosis in the FADD-deficient cells rapidly triggered a 15-fold in ATP accumulation that peaked at 4 hours and then declined (Fig. 4C-ii), while the ATP + ADP + AMP accumulation continued to increase until 8 hours (Fig. 4C-i). This robust accumulation of extracellular adenine nucleotides (Fig. 4C-i and ii) during TNF α plus BV6-induced necroptosis of the FADD-deficient cells contrasted with the near-complete absence of adenine nucleotide accumulation (Fig. 4B-i and ii) during Etop-induced apoptosis in the same FADD-deficient background.

Thus, markedly different profiles of extracellular nucleotide accumulation can occur in a given cancer cell lineage depending on the modes of regulated cell death. Notably, APCP modestly increased the ATP + ADP + AMP accumulated by TNF plus BV6-treated FADD-deficient Jurkat cells

(data not shown); this indicates that up-regulated CD73 also enhances extracellular AMP \rightarrow adenosine conversion during necroptosis.

Apoptotic Signaling and Panx1 Channel Activation in RIP1-Deficient Jurkat Cancer Cells Are Also Uncoupled from Accumulation of Extracellular Adenine Nucleotides. RIP1 plays a central role in directing TNF/TRAIL-family receptor signaling along the cell survival, extrinsic apoptotic, or necroptotic pathways (Fig. 1A). However, RIP1/FADD/caspase-8 ripoptosome complexes can also assemble during intrinsic apoptosis triggered by chemotherapeutic drugs (Tenev et al., 2011). Given the striking phenotypic effects of FADD-deletion on modulating extracellular adenine nucleotide accumulation driven by proapoptotic chemotherapeutic drugs, we tested whether deficiency in RIP1, as another ripoptosome component, results in a similar phenotype.

We induced extrinsic or intrinsic apoptosis in RIP1-deficient Jurkat cells (and WT cells as matched controls) with anti-Fas for 4 hours, STS for 4 hours, or Etop for 12 hours, respectively. RIP1-deficient Jurkat cells were characterized by the complete absence of detectable ATP + ADP + AMP accumulation in the extracellular medium during apoptotic induction by STS (Fig. 5A), Etop (Fig. 5B), or anti-Fas (Fig. 5C). Western blot analysis indicated identical caspase-3-mediated processing of both Panx1 and PARP in the WT and RIP1-deficient cells treated with STS or Etop (Fig. 5D). Similar to the FADD-deficient cells (Fig. 3E), there was no obvious alteration in mitochondrial localization in RIP1-deficient Jurkat cells before or after apoptotic induction with STS (Fig. 5E). Likewise, analysis of YO-PRO²⁺ dye influx (Figs. 5F and 5G) or calcein⁴⁻ efflux (Fig. 5H) revealed similarly robust Panx1 channel functional activity in both the WT and RIP1-deficient cells during apoptotic progression.

Ecto-AMPase Activity, but Not CD73 Expression, Is Increased in RIP1-Deficient Jurkat Cells. Given the similar phenotypes of the RIP1-deficient and FADD-deficient Jurkat cells, we tested whether the APCP inhibitor of CD73 would also rescue the ability of STS to induce accumulation of extracellular ATP + ADP + AMP in the RIP1-deficient cells. Surprisingly, inclusion of 50 μ M APCP during the STS treatment did not facilitate increased ATP + ADP + AMP accumulation in these Jurkat cells in contrast to its effects in the FADD-deficient line (Fig. 6A). We then used the same ecto-AMPase assay described for Fig. 4F to compare the abilities of the WT and RIP1-deficient cells (at identical cytocrits of 2×10^6 cells/ml) to metabolize an exogenous pulse of 1 μ M AMP in the absence or presence of 50 μ M APCP (Fig. 6B). The RIP1-deficient cells completely hydrolyzed this exogenous AMP within 30 minutes even in the presence of APCP; this contrasted with the respective 10%–20% AMP clearance activities (inhibitably by APCP) of the WT cells. Notably, qRT-PCR analysis revealed 10-fold lower levels of CD73 mRNA in these cells relative to WT Jurkat cells (Fig. 6C). This contrasted with the 5-fold higher (relative to WT) levels of CD73 mRNA in the FADD-deficient cells (Fig. 4E). Taken together, these findings indicate that RIP1-deficient

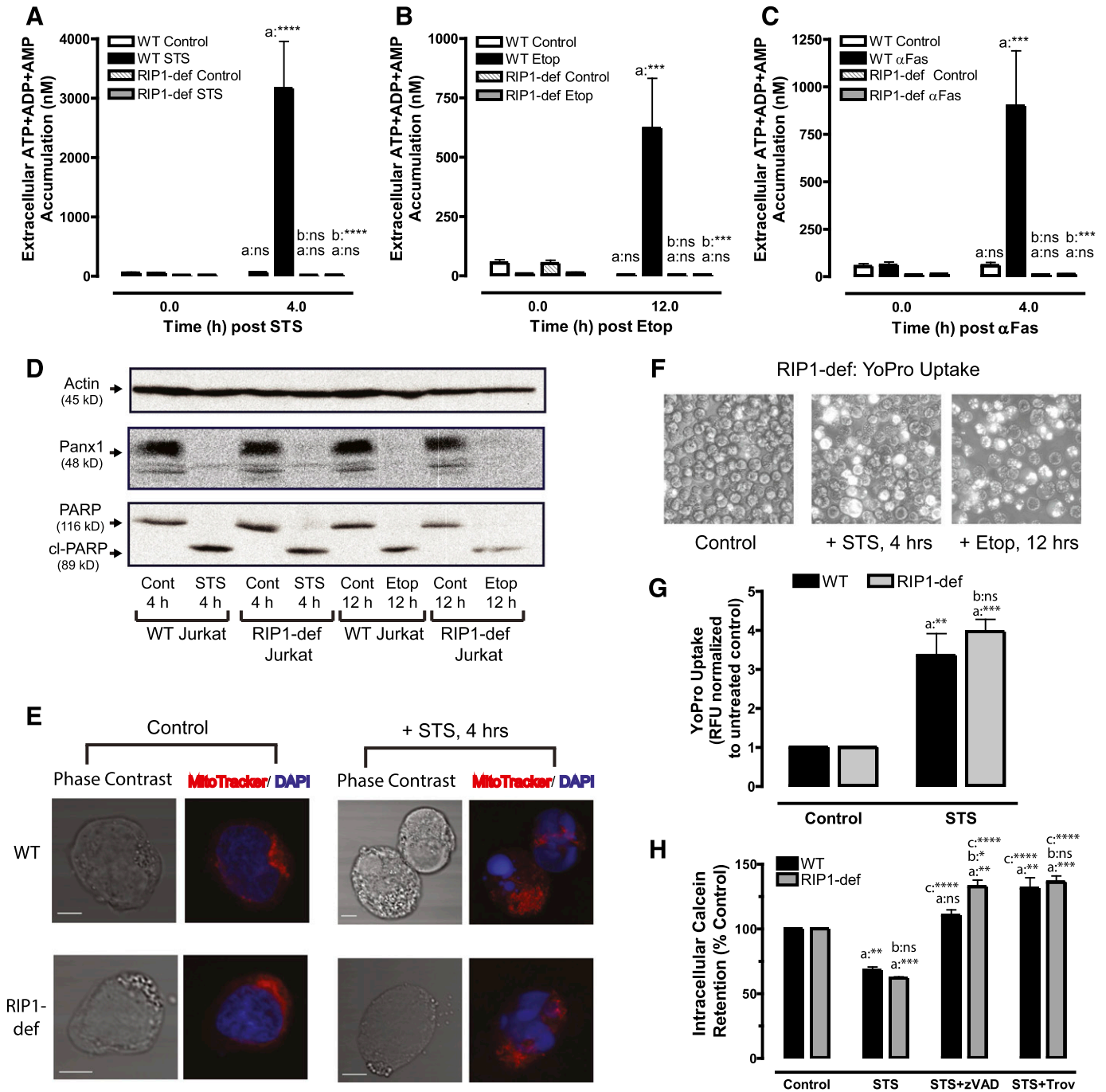


Fig. 5. Apoptotic signaling and Panx1 channel activation in RIP1-deficient Jurkat cancer cells is also uncoupled from accumulation of extracellular adenine nucleotides. (A–C) WT and RIP1-deficient Jurkat cells were treated with 3 μ M STS for 4 hours (A), 20 μ M Etop for 12 hours (B), or 250 ng/ml α Fas for 4 hours (C). Conditioned extracellular media samples were collected and assayed for total ATP + ADP + AMP accumulation. Data indicate mean \pm S.E. for three independent experiments. Analysis by two-way analysis of variance and Tukey post-test comparison; *a*: post-incubation ATP + ADP + AMP versus background ATP + ADP + AMP at time 0; *b*: RIP1-def versus WT. (D) WT or RIP1-deficient cells were treated with STS or Etop as described before preparation of whole-cell lysates for SDS-PAGE and Western blot analysis of Panx1, PARP, and actin. Data are representative of three experiments. (E) WT and RIP1-deficient Jurkat cells were treated with STS for 4 hours and then stained with MitoTracker Red and DAPI. Cells were imaged by confocal microscopy at a 60 \times magnification. Data are representative images of *n* = 15–19 individual cells. (F) RIP1-deficient cells were treated with STS or Etop for 4 or 12 hours, respectively, and cell suspensions were analyzed for YO-PRO²⁺ accumulation. Representative phase-contrast and epifluorescence microscopy images from three experiments. (G) WT and RIP1-deficient Jurkat cells were treated with 3 μ M STS for 4 hours and then washed and resuspended in BSS supplemented with 1 μ M YO-PRO²⁺; the cell suspensions were incubated for 20 minutes before quantification of YO-PRO fluorescence per well. Data indicate mean \pm S.E. from three independent experiments. Analysis by two-way analysis of variance and Tukey post-test comparison; *a*: +STS versus –STS; *b*: RIP1-def versus WT. (H) WT and RIP1-deficient Jurkat cells were loaded with 1 μ M calcein-AM and then treated with STS for 4 hours in the presence or absence of 100 μ M zVAD or 50 μ M Trova. Cells were then washed and resuspended in BSS, and calcein⁴⁻ fluorescence was measured. Data indicate mean \pm S.E. from three independent experiments. Analysis by two-way analysis of variance and Tukey post-test comparison; *a*: +STS versus –STS; *b*: RIP1-def versus WT; *c*: +STS with zVAD or Trova versus +STS alone. All panels: ns, not statistically significant; **P* < 0.05; ***P* < 0.01; ****P* < 0.001; *****P* < 0.0001.

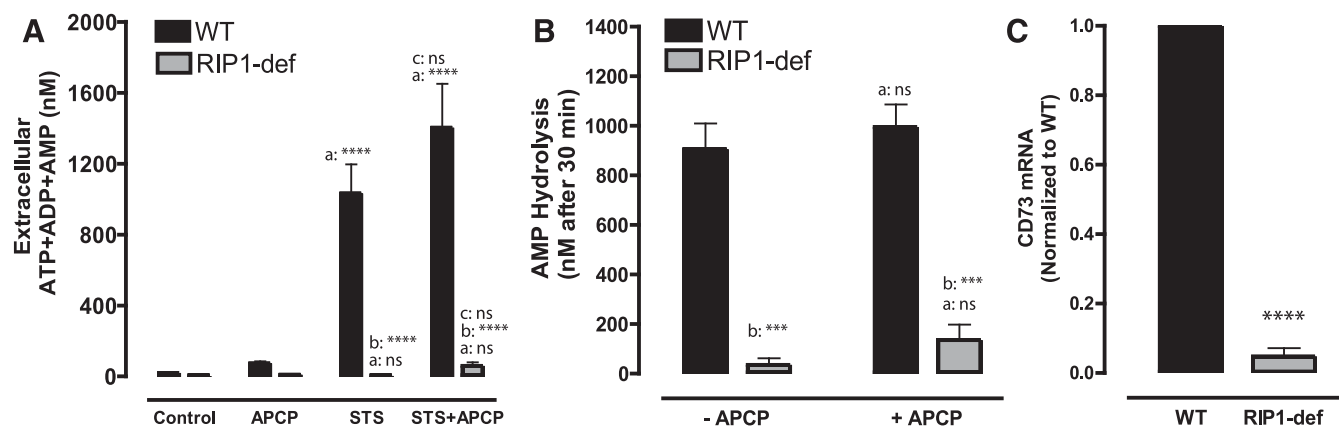


Fig. 6. Ecto-AMPase activity, but not CD73 expression, is increased in RIP1-deficient Jurkat cells. (A) WT or RIP1-deficient Jurkat cells were treated without or with STS for 4 hours in the presence or absence of 50 μ M APCP. Extracellular media samples were collected and analyzed for total ATP + ADP + AMP. Data indicate mean \pm S.E. of six independent experiments with WT cells and five independent experiments with RIP1-def cells. Analysis by two-way analysis of variance and Tukey post-test comparison; *a*: +STS versus -STS; *b*: RIP1-def versus WT; *c*: +STS with APCP versus STS alone. (B) WT or RIP1-deficient cells were suspended at 2×10^6 /ml. We added 1 μ M exogenous AMP in the presence or absence of 50 μ M APCP, and cell-free supernatants were collected after 30 minutes and analyzed for remaining [AMP]. Data indicate mean \pm S.E. of four independent experiments with WT cells and three independent experiments with RIP1-def cells. Analysis by two-way analysis of variance and Tukey post-test comparison; *a*: +APCP versus -APCP; *b*: RIP1-def versus WT. (C) qRT-PCR analysis of CD73 mRNA expression in WT and RIP1-deficient cells. Signals in RIP1-def were normalized to signals in WT and represent values from three independent experiments; analysis by two-tailed *t* test. All panels: ns, not statistically significant; ****P* < 0.001; *****P* < 0.0001.

Jurkat cells up-regulate ectoenzymes other than CD73 for robust clearance of the extracellular AMP released during intrinsic or extrinsic apoptosis.

Increased Ecto-AMPase Activity in RIP1-Deficient Jurkat Cells Correlates with Up-regulation of PAP.

Three additional ectoenzymes that can metabolize extracellular AMP are AMP deaminase, tissue nonselective alkaline phosphatase (TNAP) and PAP (Fig. 7A and Table 1). AMP deaminase, which has been described in extracellular neuromuscular synaptic junctions (Magalhães-Cardoso et al., 2003), catalyzes conversion of AMP to IMP, is distinct from adenosine deaminase, and can be inhibited by pentostatin/deoxycoformycin (Matsumoto et al., 1979; Fishbein et al., 1981; Zabielska et al., 2015). TNAP acts as a potent ecto-AMPase in some tissues and can be inhibited by levamisole or tetramisole (Picher et al., 2003; Millán, 2006). A transmembrane variant of prostatic acid phosphatase can also function as an ectonucleotidase sensitive to inhibition by L-tartrate (Quintero et al., 2007; Zylka et al., 2008; Araujo and Vihko, 2013). Extracellular adenosine may be further metabolized to inosine by adenosine deaminase, and both adenosine and inosine may be transported into cells via multiple nucleoside transporters.

We used reversed-phase HPLC to compare the metabolic fate of exogenous AMP (100 μ M) added to control WT versus RIP1-deficient Jurkat cells (Fig. 7B-i). Consistent with their low ecto-AMPase activity (Figs. 4F and 6B), the control Jurkat cells converted little of the added AMP to adenosine during the 30-minute test incubation. Although the RIP1-deficient cells catabolized most of the added AMP, no accumulation of IMP or adenosine and only a minor increase in inosine were observed. Inclusion of dipyridamole, which broadly inhibits most nucleoside transporters, did not increase accumulation of extracellular adenosine by the AMP-treated control Jurkat cells but slightly increased extracellular inosine (Fig. 7B-ii). In contrast, dipyridamole greatly increased accumulation of inosine and modestly elevated adenosine during hydrolysis of the added AMP by RIP1-deficient Jurkat cells.

This ability of the RIP1-deficient cells to rapidly metabolize extracellular AMP to inosine might occur by either of two

coupled reactions: 1) hydrolysis of AMP to adenosine followed by deamination of adenosine to inosine; or 2) deamination of AMP to IMP followed by hydrolysis of IMP to inosine (Fig. 7A). The absence of any intermediate IMP accumulation (Fig. 7B-i) during AMP clearance by the RIP1-deficient cells argued against primary AMP deamination. However, generated IMP might also be rapidly hydrolyzed by a coexpressed ectonucleotidase.

We attempted to test whether pentostatin would attenuate AMP \rightarrow inosine conversion via the AMP deamination pathway, but elution of pentostatin (which is a nucleoside analog) broadly overlapped with IMP and AMP in the employed HPLC protocol. However, using the enzyme-based AMP assay we were unable to observe a suppressive effect of pentostatin on the rapid clearance of exogenously added AMP by the RIP1-deficient Jurkat cells (data not shown). Pentostatin also failed to facilitate increased accumulation of extracellular ATP + ADP + AMP during STS-induced apoptosis of the RIP1-deficient cells (Fig. 7C).

Taken together, these results argue against a major role for an ecto-AMP deaminase in this mutant Jurkat cell line. Interestingly, pentostatin modestly increased the extracellular ATP + ADP + AMP accumulation by STS-treated WT Jurkat cells (Fig. 7C). This may reflect increased availability of intracellular AMP, for efflux via Panx1, due to suppression of intracellular AMP deaminase by pentostatin that is readily accumulated via nucleoside transporters.

The TNAP inhibitor tetramisole did not prevent the rapid AMP clearance by RIP1-deficient Jurkat cells (data not shown). Likewise, inclusion of tetramisole during STS-induced apoptosis of these cells failed to rescue extracellular accumulation of ATP + ADP + AMP (data not shown). Thus, increased TNAP expression does not underlie the robust ecto-AMPase activity of the RIP1-deficient cells.

To offset the complication of the three coupled reactions (AMP hydrolysis, adenosine deamination, inosine uptake) in the RIP1-deficient Jurkat line, we incubated these cells (and WT Jurkat cells as a control) with 10 μ M ϵ -AMP and measured both its decrease and the corresponding increase in ϵ -ADO by

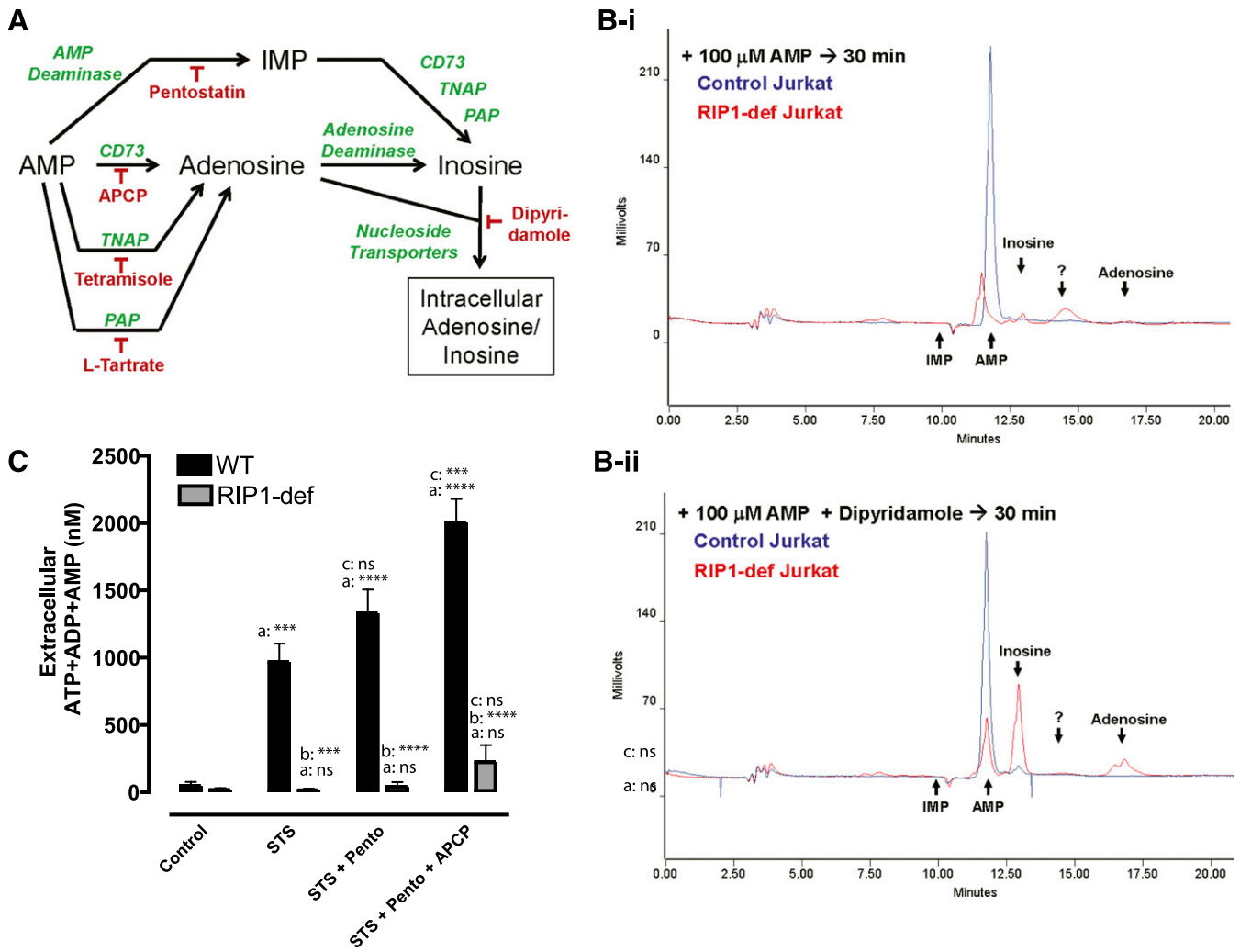


Fig. 7. Increased ecto-AMPase activity of RIP-deficient Jurkat cells is not correlated with up-regulation of ecto-AMP deaminase. (A) Schematic of extracellular pathways, ectoenzymes (green), and inhibitors (red) that can mediate the metabolism/clearance of released AMP. (B) We added 100 μ M AMP minus (B-i, upper traces) or plus (B-ii, lower traces) 50 μ M dipyridamole to WT or RIP1-deficient cells (2×10^6 cells/ml in BSS + 5 mM glucose + 0.1% BSA). Cell-free supernatants were collected after 30 minutes and processed for separation and quantification of AMP, IMP, adenosine, and inosine by reverse phase HPLC and absorbance detection. Arrows indicate elution times of AMP, IMP, adenosine, and inosine standards; ? indicates an unidentified peak. Data are representative of four to six experiments. (C) WT or RIP1-deficient Jurkat cells were treated without or with STS for 4 hours in the presence or absence of 50 μ M APCP, 200 μ M pentostatin, or combined APCP plus pentostatin. Data indicate mean \pm S.E. of three independent experiments. Analysis by two-way analysis of variance and Tukey post-test comparison; a: +STS versus -STS; b: RIP1-def versus WT; c: +STS with pentostatin or pentostatin plus APCP versus STS alone. All panels: ns, not statistically significant; * $P < 0.05$; ** $P < 0.01$; *** $P < 0.001$; **** $P < 0.0001$.

anion exchange HPLC and fluorescence detection (Fig. 8A). Etheno-modification of the adenine moiety on AMP or adenosine prevents their use by deaminases but not by CD73 or other ecto-AMPases (Jamal et al., 1988; Bonitati et al., 1993). Additionally, ϵ -ADO is a poor substrate for nucleoside transporters. Figure 8A demonstrates that ecto- ϵ -AMPase activity in RIP1-deficient Jurkat cells is 8- to 10-fold higher than in the WT line; it is also 4- to 5-fold greater than in the FADD-deficient line (data not shown). Consistent with the enzyme-based assay of extracellular AMP clearance, tetramisole did not suppress the robust ϵ -AMP \rightarrow ϵ -ADO conversion by the RIP1-deficient cells while APCP only modestly decreased this reaction (data not shown).

Prostatic acid phosphatase, encoded by the *ACPP* gene, is a canonical marker of human prostate cancer (Araujo and Vihko, 2013). Multiple *ACPP* splice variants yield a secreted PAP isoform and another with a transmembrane anchor (TM-PAP). Recent studies have indicated that TM-PAP mRNA and

enzyme activity is expressed in normal murine and human lymphoid tissues and different T-cell subsets (Quintero et al., 2007; Yegutkin et al., 2014). Notably, inclusion of 10 mM L-tartrate, as a low affinity but high-efficacy inhibitor of PAP isoforms, markedly ($\sim 80\%$) attenuated the robust ϵ -AMP \rightarrow ϵ -ADO metabolism by the RIP1-deficient Jurkat cells (Fig. 8B).

Although short-term treatment of intact cells with L-tartrate can be used to assess the contribution of TM-PAP to hydrolysis of exogenously added AMP or ϵ -AMP, prolonged treatment is cytotoxic. Thus, we were unable to test whether L-tartrate might rescue extracellular ATP + ADP + AMP accumulation during STS-induced apoptosis of RIP1-deficient Jurkat cells. However, we assessed the ability of these cells, as well as the WT and FADD-deficient Jurkat cells, to hydrolyze extracellular *p*-nitrophenyl phosphate (as a non-nucleotide substrate of PAP enzymes) under physiologic (pH 7.5) or acidotic (pH 6.5) conditions (Fig. 8C).

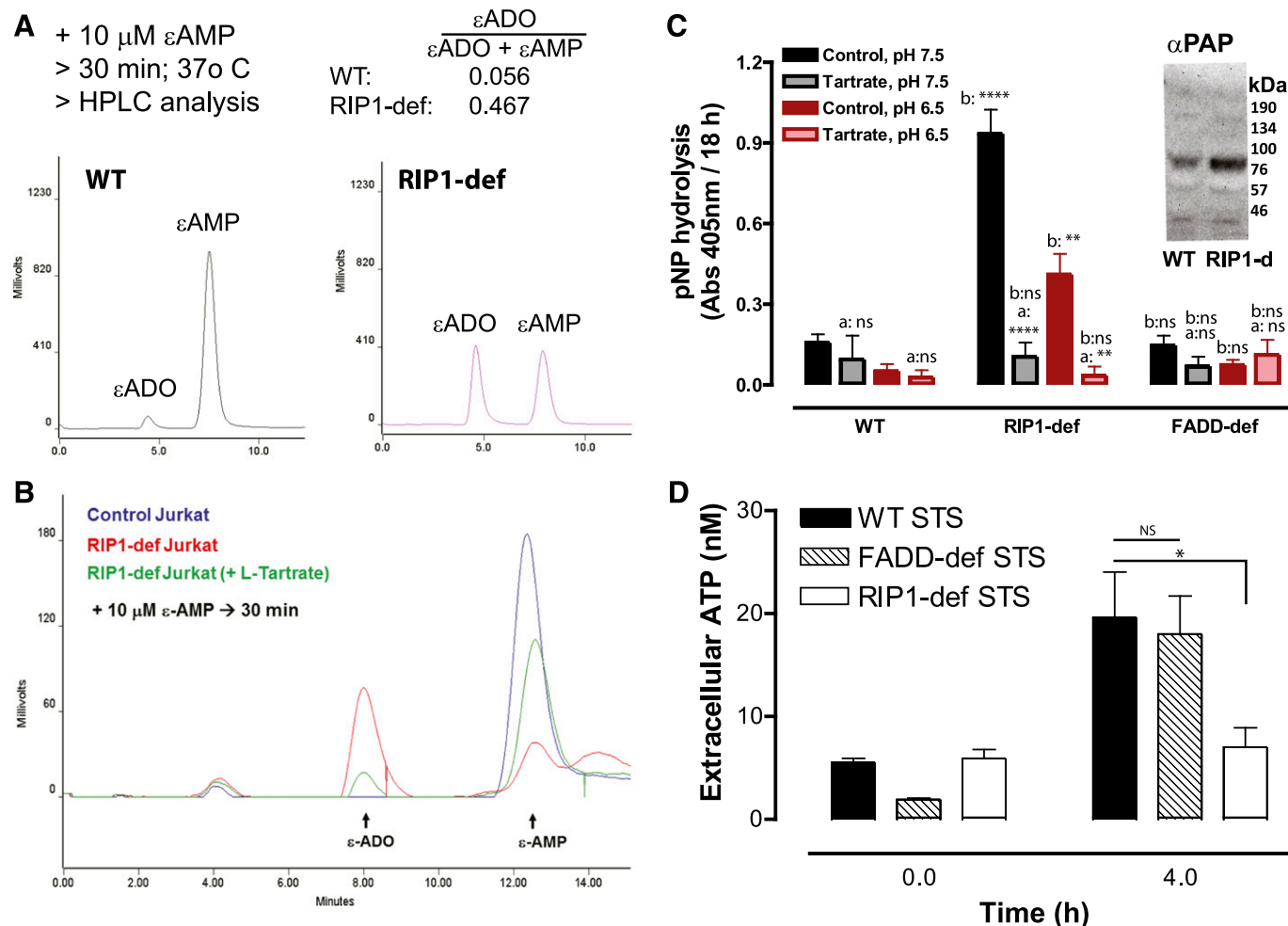


Fig. 8. Increased ecto-AMPase activity in RIP1-deficient Jurkat cells correlates with up-regulation of PAP. (A) 10 μM $\epsilon\text{-AMP}$ was added to WT or RIP1-deficient cells (2×10^6 cells/ml). Cell-free supernatants were collected after 30 minutes and processed for separation and quantification of $\epsilon\text{-ADO}$ and $\epsilon\text{-AMP}$ by anion exchange HPLC and fluorescence detection. Data are representative of three experiments. (B) We added 10 μM $\epsilon\text{-AMP}$ to WT or RIP1-deficient cells (2×10^6 cells/ml) in the absence or presence of 10 mM L-tartrate. Cell-free supernatants were collected after 30 minutes and processed for separation and quantification of $\epsilon\text{-ADO}$ and $\epsilon\text{-AMP}$ by anion exchange HPLC and fluorescence detection. Data are representative of four experiments. (C) WT, RIP1-deficient, or FADD-deficient Jurkat cells (2×10^6 /ml) were plated in 96-well plates and suspended in BSS that was buffered to pH 7.5 or pH 6.5. The cell suspensions were supplemented with 500 μM *p*-nitrophenyl phosphate in the absence or presence of 10 mM L-tartrate and incubated for 18 hours at 25 $^{\circ}\text{C}$. Hydrolysis of *p*-nitrophenyl phosphate to nitrophenyl was assayed by measuring absorbance at 405 nm. Data indicate mean \pm S.E. of three independent experiments. Analysis by two-way analysis of variance and Tukey post-test comparison. *a*: +tartrate versus -tartrate; *b*: RIP1-def or FADD-def versus WT. (C, inset) Western blot analysis of PAP expression in whole-cell lysates from WT or RIP1-deficient Jurkat cells that were resolved by SDS-PAGE and transferred to polyvinylidene fluoride membranes; mobility of molecular mass markers is indicated on the right. (D) WT, FADD-deficient, and RIP1-deficient Jurkat cells were treated with 3 μM STS for 4 hours. Extracellular media samples were collected and assayed for extracellular ATP. Data indicate mean \pm S.E. of three independent experiments. Analysis by two-way analysis of variance and Tukey post-test comparison. All panels: ns, not statistically significant; * $P < 0.05$; ** $P < 0.01$; **** $P < 0.0001$.

Hydrolysis of *p*-nitrophenyl phosphate by RIP1-deficient Jurkat cells was \sim 8-fold higher than in the WT or FADD-deficient Jurkat cells at either pH 7.5 or 6.5. Importantly, this phosphatase activity was markedly inhibited by L-tartrate (Fig. 8C) but not the APCP inhibitor of CD73 (data not shown). Interestingly, Western blot analysis with an antibody that recognizes both the secreted and transmembrane forms of PAP revealed an immunoreactive band (\sim 70 kDa) in whole-cell lysates from both RIP1-deficient and WT Jurkat cells, albeit with stronger intensity in the RIP1-deficient cells.

Because TM-PAP has a lysosomal sorting signal, it can traffic to both the lysosomal and plasma membrane compartments. The large difference in ecto-phosphatase activity between the control and RIP1-deficient cells suggests that TM-PAP may be retained in lysosomes of control Jurkat cells

while predominantly trafficking to the surface membrane of the RIP1-deficient cells. Taken together, these observations suggest that the membrane-anchored variant of PAP is markedly up-regulated in RIP-deficient Jurkat cells to function as the robust ecto-AMPase activity that defines these leukemic T cells.

As noted previously, the initial phases of STS-stimulated extracellular ATP accumulation (Fig. 4A-ii) were similar in the WT and FADD-deficient Jurkat cells despite marked differences in total ATP + ADP + AMP accumulation (Fig. 4A-i). We compared STS-stimulated extracellular ATP accumulation in WT, FADD-deficient, and RIP-deficient Jurkat cells and observed markedly reduced extracellular ATP accumulation in the RIP-deficient cells relative to the other two Jurkat lines (Fig. 8D). This is consistent with the reported

ability of TM-PAP to directly metabolize ATP in addition to AMP (Table 1). Because CD39 expression is very low in WT Jurkat cells (Yegutkin et al., 2006; Chekeni et al., 2010; Boyd-Tressler et al., 2014), we also compared ecto-ATPase activity levels in WT versus RIP-deficient Jurkat cells incubated with 1 μ M exogenous ATP for 30 minutes in the absence or presence of the CD39 inhibitor ARL-67156 (ARL). While WT cells hydrolyzed only 5% of the ATP, the RIP1-deficient cells cleared ~45% of the ATP, and this was partially inhibited (by ~50%) by ARL (data not shown). Thus, increased TM-PAP and CD39 activity in RIP1-deficient Jurkat cells likely contributes to their decreased ability to accumulate extracellular ATP during STS-induced apoptosis (Fig. 8D).

Discussion

This study provides new insights regarding mechanisms of adenine nucleotide release and extracellular metabolism by cancer cells (Jurkat human leukemic T cells) during different modes of regulated cell death. First, we extended previous findings (Chekeni et al., 2010; Boyd-Tressler et al., 2014) verifying the critical role of caspase-3-activated Panx1 channels as an ATP/AMP efflux pathway to cells undergoing extrinsic apoptosis in response to the TNFR1 member of the Fas/TNFR/TRAIL death receptor family. Second, we demonstrated that redirection of TNFR1 signaling from apoptosis to necroptosis results in redirection of the ATP efflux mechanism from opening of Panx1 channels to insertion of RIP3-phosphorylated MLKL pores into the plasma membrane. Third, we observed that, due to its rapid *intracellular* production during both apoptotic and necroptotic progression, AMP becomes a major nucleotide substrate for both Panx1 channels and MLKL pores, resulting in its robust *extracellular* accumulation during both modes of regulated cell death. Finally, we found that genetic ablation of FADD and RIP1, two critical adapter proteins for TNFR/TRAIL death receptor signaling, uncouples caspase-3-activated Panx1 channels from extracellular adenine nucleotide accumulation due to up-regulated expression of diverse ectonucleotidases. These included the CD73 ecto-AMPase in FADD-deficient Jurkat cells versus a membrane-anchored prosthetic acid phosphatase (TM-PAP) ecto-AMPase in the RIP1-deficient Jurkat cells. This provides insight into how regulation of extracellular ATP, AMP, and adenosine levels may vary during expansion of clonal variants of a given cancer cell type.

TNFR1 can signal through different pathways in cancer cells (Fig. 1A). TNFR1 activation of BV6-treated WT Jurkat cells induced an increase in extracellular adenine nucleotides over 12 hours (after an initial 2-hour lag phase). This accumulation was mediated by active Panx1 channels in the absence of overt cell lysis. These responses to TNF α recapitulated those elicited by Fas activation but with slower kinetics. Notably, adenine nucleotide release in response to TNF α /BV6 was completely redirected from Panx1 channels to MLKL pores in Jurkat cells lacking expression of FADD.

Other studies have described the release of ATP during necroptotic progression in human THP-1 monocytic leukemia cells (Wang et al., 2015) and a human bronchial epithelial cell line (Pouwels et al., 2016). These reports noted that conditioned media from the necroptotic cells stimulated the P2Y receptor-mediated migration of phagocytic leukocytes similar to earlier studies using conditioned medium from apoptotic Jurkat cells (Elliott et al., 2009; Chekeni et al., 2010). Our

studies support a model whereby released ATP acts as a major “find-me” signal for phagocytic leukocytes to migrate toward either apoptotic or necroptotic tumor cells as a prelude to tumor cell clearance and processing of tumor antigens for presentation to T cells.

Most studies of nucleotide release from dying cancer cells focus on extracellular accumulation of ATP, given its roles as a find-me ligand for directed migration of phagocytes and a proimmunogenic mediator (Elliott et al., 2009; Ghiringhelli et al., 2009; Martins et al., 2009, 2014; Chekeni et al., 2010; Michaud et al., 2011; Ma et al., 2013). However, both Panx1 channels (Chiu et al., 2014) and MLKL pores (Dondelinger et al., 2014; Galluzzi et al., 2014; Su et al., 2014) are defined by broad permeability to organic/inorganic anions and cations with molecular masses in the 1000 Da range or smaller. These will include nucleotides other than ATP, such as UTP, which also acts as a find-me ligand (Chekeni et al., 2010; Lazarowski, 2012), and intracellular metabolites of ATP, such as AMP (Boyd-Tressler et al., 2014; Yamaguchi et al., 2014).

Our study extends previous findings that AMP becomes the predominant nucleotide released via Panx1 channels during the progression of apoptotic execution. AMP, in addition to ATP, was also increasingly released via MLKL pores during necroptotic progression in TNF α /BV6-stimulated FADD-deficient Jurkat cells. Earlier studies determined that the intracellular nucleotide pool of apoptotic cells shifts from an initially high [ATP] to progressively lower [ATP] as a consequence of increased ATP utilization and decreased mitochondrial ATP synthesis (Waterhouse et al., 2001; Ricci et al., 2004). This was linked to the caspase-3-mediated cleavage and inactivation of the p75 subunit of complex I of the electron transport chain (Ricci et al., 2004).

A decrease in the cytosolic [ATP]/[AMP] ratio likely also occurs during necroptosis. Using TNF α /BV6 stimulated-FADD-deficient Jurkat cells, Schenk and Fulda (2015) observed that necroptotic progression is facilitated by a positive feedback loop whereby activated MLKL promotes accumulation of mitochondrial reactive oxygen species, which in turn further stabilize formation of RIP1/RIP3 necrosomes. Such diversion of mitochondrial function to reactive oxygen species production will decrease ATP production, while insertion of MLKL pores into the plasma will increase ATP breakdown to ADP and AMP as a result of increased Na⁺, K⁺-ATPase, and Ca²⁺-ATPase activity secondary to enhanced Na⁺ influx (Chen et al., 2014) and Ca²⁺ influx (Cai et al., 2014) mediated by MLKL pores.

An increasing accumulation of AMP in the *in vivo* extracellular microenvironment of apoptotic or necroptotic tumor cells is significant due to its modulatory effects on proimmunogenic and proinflammatory signaling. In contrast to ATP, AMP is not an agonistic ligand for the immunostimulatory P2 receptors expressed on phagocytic leukocytes or tumor antigen-reactive T cells. Rather, extracellular AMP is a potential source for the production of adenosine, which activates the immunosuppressive A2a/ A2b adenosine receptors expressed on those leukocytes and T cells. This potential capacity of extracellular AMP to drive local accumulation of immunosuppressive adenosine will be determined by the relative expression of various ecto-AMPases on the tumor cells per se, adjacent stromal cells, and recruited leukocytes.

Altered expression or mutation of proapoptotic or pronecroptotic signaling proteins contributes to tumor cell resistance to chemotherapeutic agents. We verified efficient

intrinsic apoptosis in FADD-deficient or RIP1-deficient Jurkat cells treated with STS or Etop, two mechanistically distinct proapoptotic drugs. Despite efficient gating of Panx1 channels in apoptotic FADD-deficient or RIP1-deficient Jurkat cells, little or no extracellular adenine nucleotide accumulation was observed. This uncoupling of Panx1 channel activity from adenine nucleotide accumulation was linked to increased expression of CD73 ecto-AMPase in the FADD-deficient Jurkat line, but up-regulation of TM-PAP as a robust ecto-AMPase in the RIP1-deficient Jurkat line.

Only a 2-fold increase in CD73 activity distinguished the FADD-deficient cells from the WT cells, but this was sufficient to markedly reduce AMP accumulation during apoptosis. The modest increase in CD73 activity also suppressed extracellular ATP accumulation in response to Etop but not STS. This suggests that increased clearance of extracellular AMP by CD73 may relieve product inhibition of the upstream CD39 ecto-ATPase and thereby result in increased clearance of ATP if the latter is delivered to the extracellular compartment at a relatively slow rate. Indeed, the increased CD73 activity of FADD-deficient Jurkat cells was insufficient to prevent accumulation of AMP or ATP during TNF α /BV6-induced necroptosis. This implies that the rate of efflux of ATP and AMP via activated MLKL pores exceeds the rate of AMP clearance by up-regulated CD73. Importantly, the CD73 inhibitor APCP rescued the apoptotic adenine nucleotide accumulation responses in the FADD-deficient cells and further enhanced necroptotic adenine nucleotide accumulation.

The absence of RIP1 expression in Jurkat cells resulted in an even more dramatic suppression of the adenine nucleotide accumulation responses during intrinsic or extrinsic apoptosis. Although the RIP1-deficient Jurkat line was characterized by a ~10-fold greater ecto-AMPase activity relative to the parental control Jurkat cell line, this was not mediated by CD73. Pharmacologic approaches and HPLC-based assays of extracellular AMP metabolism ruled out contributions of tissue nonselective alkaline phosphatase and extracellular AMP deaminases. Rather, we determined that a remarkable up-regulation of an L-tartrate-sensitive TM-PAP was responsible for rapid clearance of released nucleotides.

Despite its canonical association with the prostate gland, recent studies have indicated that TM-PAP and/or the secreted PAP isoform function as significant ectonucleotidases in multiple tissues and cell types, including saliva (Araujo et al., 2014), dorsal root ganglion neurons that mediate nociception (Street et al., 2011; Zylka et al., 2008), and normal T lymphocytes (Yegutkin et al., 2014). Up-regulated PAP is also used as a biomarker of prostate cancer (Hakalahti et al., 1993), and our observations suggest the possibility that it may also be a marker for some subtypes of leukemias. Because selective and well-defined pharmacologic inhibitors of PAP ectonucleotidase activity are not readily available (Larsen et al., 2009; McCoy et al., 2013), most studies have used PAP-knockout mice to define physiologic roles (Zylka et al., 2008; Street et al., 2011; Yegutkin et al., 2014). Studies using siRNA with Jurkat cells and other human leukemia lines would be informative to define roles for TM-PAP in the growth, survival, and immunogenicity of hematopoietic tumors.

In contrast to ATP, AMP is not an agonist for immunostimulatory P2 nucleotide receptors but is a substrate for production of immunosuppressive adenosine. Because WT Jurkat cells are defined by low rates of ATP and AMP hydrolysis, even modest increases in CD73 or TM-PAP altered

the extracellular balance of ATP versus adenosine and may attenuate tumor immunogenicity. The mechanisms whereby altered FADD or RIP expression modulate CD73 and TM-PAP expression are unclear. However, differential expression of CD73 or TM-PAP in clonal tumor variants may determine whether chemotherapeutic drug-induced activation of Panx1 channels predominantly drive accumulation of immunostimulatory ATP versus immunosuppressive adenosine.

Acknowledgments

The authors thank Silva Penuela and Dale Laird (University of Western Ontario, ON Canada) for providing the anti-human pannexin-1 antisera.

Author Contributions

Participated in research design: Boyd-Tressler, Dubyak.
Conducted experiments: Boyd-Tressler, Lane, Dubyak.
Performed data analysis: Boyd-Tressler, Dubyak.
Wrote or contributed to the writing of the manuscript: Boyd-Tressler, Dubyak.

References

- Antonioni L, Blandizzi C, Pacher P, and Haskó G (2013a) Immunity, inflammation and cancer: a leading role for adenosine. *Nat Rev Cancer* **13**:842–857.
- Antonioni L, Pacher P, Vizi ES, and Haskó G (2013b) CD39 and CD73 in immunity and inflammation. *Trends Mol Med* **19**:355–367.
- Araujo CL, Quintero IB, Kipar A, Herrala AM, Pulkka AE, Saarinen L, Hautaniemi S, and Vihko P (2014) Prostatic acid phosphatase is the main acid phosphatase with 5'-ectonucleotidase activity in the male mouse saliva and regulates salivation. *Am J Physiol Cell Physiol* **306**:C1017–C1027.
- Araujo CL and Vihko PT (2013) Structure of acid phosphatases. *Methods Mol Biol* **1053**:155–166.
- Beavis PA, Stagg J, Darcy PK, and Smyth MJ (2012) CD73: a potent suppressor of antitumor immune responses. *Trends Immunol* **33**:231–237.
- Belz K, Schoeneberger H, Wehner S, Weigert A, Bönig H, Klingebiel T, Fichtner I, and Fulda S (2014) Smac mimetic and glucocorticoids synergize to induce apoptosis in childhood ALL by promoting ripoptosome assembly. *Blood* **124**:240–250.
- Bhattarai S, Freundlieb M, Pippel J, Meyer A, Abdelrahman A, Fiene A, Lee SY, Zimmermann H, Yegutkin GG, Sträter N, et al. (2015) α,β -Methylene-ADP (AOPCP) derivatives and analogues: development of potent and selective ecto-5'-nucleotidase (CD73) inhibitors. *J Med Chem* **58**:6248–6263.
- Bonitai AE, Agarwal KC, and Rounds S (1993) A simple assay for ecto-5'-nucleotidase using intact pulmonary artery endothelial cells. Effect of endotoxin-induced cell injury. *Biochem Pharmacol* **46**:1467–1473.
- Bono MR, Fernández D, Flores-Santibáñez F, Roseblatt M, and Sauma D (2015) CD73 and CD39 ectonucleotidases in T cell differentiation: beyond immunosuppression. *FEBS Lett* **589**:3454–3460.
- Boyd-Tressler A, Penuela S, Laird DW, and Dubyak GR (2014) Chemotherapeutic drugs induce ATP release via caspase-gated pannexin-1 channels and a caspase/pannexin-1-independent mechanism. *J Biol Chem* **289**:27246–27263.
- Cai Z, Jitkaew S, Zhao J, Chiang HC, Choksi S, Liu J, Ward Y, Wu LG, and Liu ZG (2014) Plasma membrane translocation of trimerized MLKL protein is required for TNF-induced necroptosis. *Nat Cell Biol* **16**:55–65.
- Chekeni FB, Elliott MR, Sandilos JK, Walk SF, Kinchen JM, Lazarowski ER, Armstrong AJ, Penuela S, Laird DW, Salvesen GS, et al. (2010) Pannexin 1 channels mediate 'find-me' signal release and membrane permeability during apoptosis. *Nature* **467**:863–867.
- Chen X, Li W, Ren J, Huang D, He WT, Song Y, Yang C, Li W, Zheng X, Chen P, et al. (2014) Translocation of mixed lineage kinase domain-like protein to plasma membrane leads to necrotic cell death. *Cell Res* **24**:105–121.
- Chiu YH, Ravichandran KS, and Bayliss DA (2014) Intrinsic properties and regulation of Pannexin 1 channel. *Channels (Austin)* **8**:103–109.
- Deaglio S, Dwyer KM, Gao W, Friedman D, Usheva A, Erat A, Chen JF, Enjyoji K, Linden J, Oukka M, et al. (2007) Adenosine generation catalyzed by CD39 and CD73 expressed on regulatory T cells mediates immune suppression. *J Exp Med* **204**:1257–1265.
- Dondelinger Y, Declercq W, Montessuit S, Roelandt R, Goncalves A, Bruggeman I, Hulpiau P, Weber K, Sehon CA, Marquis RW, et al. (2014) MLKL compromises plasma membrane integrity by binding to phosphatidylinositol phosphates. *Cell Reports* **7**:971–981.
- Dzhandzhugazyan KN, Kirkin AF, thor Straten P, and Zeuthen J (1998) Ecto-ATP diphosphohydrolase/CD39 is overexpressed in differentiated human melanomas. *FEBS Lett* **430**:227–230.
- Elliott MR, Chekeni FB, Trampont PC, Lazarowski ER, Kadl A, Walk SF, Park D, Woodson RI, Ostankovich M, Sharma P, et al. (2009) Nucleotides released by apoptotic cells act as a find-me signal to promote phagocytic clearance. *Nature* **461**:282–286.
- Feoktistova M, Geserick P, Kellert B, Dimitrova DP, Langlais C, Hupe M, Cain K, MacFarlane M, Häcker G, and Leverkus M (2011) cIAPs block ripoptosome formation, a RIP1/caspase-8 containing intracellular cell death complex differentially regulated by cFLIP isoforms. *Mol Cell* **43**:449–463.
- Fishbein WN, Davis JJ, Winkert JW, and Strong DM (1981) Levels of adenosine deaminase AMP deaminase, and adenylate kinase in cultured human lymphoblast lines: exquisite sensitivity of AMP deaminase to adenosine deaminase inhibitors. *Biochem Med* **26**:377–386.

- Galluzzi L, Kepp O, and Kroemer G (2014) MLKL regulates necrotic plasma membrane permeabilization. *Cell Res* **24**:139–140.
- Ghiringhelli F, Apetoh L, Tesniere A, Aymeric L, Ma Y, Ortiz C, Vermaelen K, Panaretakis T, Mignot G, Ullrich E, et al. (2009) Activation of the NLRP3 inflammasome in dendritic cells induces IL- β -dependent adaptive immunity against tumors. *Nat Med* **15**:1170–1178.
- Gude DR, Alvarez SE, Paugh SW, Mitra P, Yu J, Griffiths R, Barbour SE, Milstien S, and Spiegel S (2008) Apoptosis induces expression of sphingosine kinase 1 to release sphingosine-1-phosphate as a “come-and-get-me” signal. *FASEB J* **22**:2629–2638.
- Hakalahti L, Vihko P, Henttu P, Autio-Harmainen H, Soini Y, and Vihko R (1993) Evaluation of PAP and PSA gene expression in prostatic hyperplasia and prostatic carcinoma using northern-blot analyses, in situ hybridization and immunohistochemical stainings with monoclonal and bispecific antibodies. *Int J Cancer* **55**:590–597.
- Hamp R (1985) Luminometric method, in *Methods of Enzymatic Analysis* (Bergmeyer HU, ed) p 370, Verlag Chemie, Weinheim.
- Humphries F, Yang S, Wang B, and Moynagh PN (2015) RIP kinases: key decision makers in cell death and innate immunity. *Cell Death Differ* **22**:225–236.
- Jamal Z, Afkham-Ebrahimi A, and Saggerson ED (1988) A novel assay for 5'-nucleotidase using 1,N ϵ -etheno-AMP as substrate, and comments on the properties of the reaction product, ethenoadenosine. *Biochem J* **250**:369–373.
- Junker C and Hoth M (2011) Immune synapses: mitochondrial morphology matters. *EMBO J* **30**:1187–1189.
- Kepp O, Tesniere A, Zitvogel L, and Kroemer G (2009) The immunogenicity of tumor cell death. *Curr Opin Oncol* **21**:71–76.
- Larsen RS, Zylka MJ, and Scott JE (2009) A high throughput assay to identify small molecule modulators of prostatic acid phosphatase. *Curr Chem Genomics* **3**:42–49.
- Lazarowski ER (2012) Vesicular and conductive mechanisms of nucleotide release. *Purinergic Signal* **8**:359–373.
- Ledderose C, Bao Y, Lidicky M, Zipperle J, Li L, Strasser K, Shapiro NI, and Junger WG (2014) Mitochondria are gate-keepers of T cell function by producing the ATP that drives purinergic signaling. *J Biol Chem* **289**:25936–25945.
- Loi S, Pommey S, Haibe-Kains B, Beavis PA, Darcy PK, Smyth MJ, and Stagg J (2013) CD73 promotes antitumor resistance and poor prognosis in triple negative breast cancer. *Proc Natl Acad Sci USA* **110**:11091–11096.
- Ma Y, Adjemian S, Yang H, Catani JP, Hannani D, Martins I, Michaud M, Kepp O, Sukkurwala AQ, Vacchelli E, et al. (2013) ATP-dependent recruitment, survival and differentiation of dendritic cell precursors in the tumor bed after anticancer chemotherapy. *Oncol Immunology* **2**:e24568.
- Magalhães-Cardoso MT, Pereira MF, Oliveira L, Ribeiro JA, Cunha RA, and Correia-de-Sá P (2003) Ecto-AMP deaminase blunts the ATP-derived adenosine A2A receptor facilitation of acetylcholine release at rat motor nerve endings. *J Physiol* **549**:399–408.
- Martinou JC and Youle RJ (2011) Mitochondria in apoptosis: Bcl-2 family members and mitochondrial dynamics. *Dev Cell* **21**:92–101.
- Martins I, Tesniere A, Kepp O, Michaud M, Schlemmer F, Senovilla L, Séror C, Métivier D, Perfettini JL, Zitvogel L, et al. (2009) Chemotherapy induces ATP release from tumor cells. *Cell Cycle* **8**:3723–3728.
- Martins I, Wang Y, Michaud M, Ma Y, Sukkurwala AQ, Shen S, Kepp O, Métivier D, Galluzzi L, Perfettini JL, et al. (2014) Molecular mechanisms of ATP secretion during immunogenic cell death. *Cell Death Differ* **21**:79–91.
- Matsumoto SS, Raivio KO, and Seegmiller JE (1979) Adenine nucleotide degradation during energy depletion in human lymphoblasts. Adenosine accumulation and adenylate energy charge correlation. *J Biol Chem* **254**:8956–8962.
- McCoy ES, Lea WA, Mott BT, Maloney DJ, Jadhav A, Simeonov A, and Zylka MJ (2013) High-throughput screen identifies cyclic nucleotide analogs that inhibit prostatic acid phosphatase. *J Biomol Screen* **18**:481–489.
- Michaud M, Martins I, Sukkurwala AQ, Adjemian S, Ma Y, Pellegatti P, Shen S, Kepp O, Scoazec M, Mignot G, et al. (2011) Autophagy-dependent anticancer immune responses induced by chemotherapeutic agents in mice. *Science* **334**:1573–1577.
- Mikhailov A, Sokolovskaya A, Yegutkin GG, Amdahl H, West A, Yagita H, Lahesmaa R, Thompson LF, Jalkanen S, Blokhin D, et al. (2008) CD73 participates in cellular multiresistance program and protects against TRAIL-induced apoptosis. *J Immunol* **181**:464–475.
- Millán JL (2006) Alkaline phosphatases: structure, substrate specificity and functional relatedness to other members of a large superfamily of enzymes. *Purinergic Signal* **2**:335–341.
- Morgan MJ, Kim YS, and Liu ZG (2009) Membrane-bound Fas ligand requires RIP1 for efficient activation of caspase-8 within the death-inducing signaling complex. *J Immunol* **183**:3278–3284.
- Nevedomskaya E, Perryman R, Solanki S, Syed N, Mayboroda OA, and Keun HC (2016) A systems oncology approach identifies NT5E as a key metabolic regulator in tumor cells and modulator of platinum sensitivity. *J Proteome Res* **15**:280–290.
- Penuela S, Bhalla R, Gong XQ, Cowan KN, Celetti SJ, Cowan BJ, Bai D, Shao Q, and Laird DW (2007) Pannexin 1 and pannexin 3 are glycoproteins that exhibit many distinct characteristics from the connexin family of gap junction proteins. *J Cell Sci* **120**:3772–3783.
- Penuela S, Bhalla R, Nag K, and Laird DW (2009) Glycosylation regulates pannexin intermixing and cellular localization. *Mol Biol Cell* **20**:4313–4323.
- Penuela S, Gehl R, and Laird DW (2013) The biochemistry and function of pannexin channels. *Biochim Biophys Acta* **1828**:15–22.
- Peter C, Waibel M, Keppeler H, Lehmann R, Xu G, Halama A, Adamski J, Schulze-Osthoff K, Wesselborg S, and Lauber K (2012) Release of lysophospholipid ‘find-me’ signals during apoptosis requires the ATP-binding cassette transporter A1. *Autoimmunity* **45**:568–573.
- Peter C, Waibel M, Radu CG, Yang LV, Witte ON, Schulze-Osthoff K, Wesselborg S, and Lauber K (2008) Migration to apoptotic “find-me” signals is mediated via the phagocyte receptor G2A. *J Biol Chem* **283**:5296–5305.
- Picher M, Burch LH, Hirsh AJ, Szychala J, and Boucher RC (2003) Ecto 5'-nucleotidase and nonspecific alkaline phosphatase. Two AMP-hydrolyzing ectoenzymes with distinct roles in human airways. *J Biol Chem* **278**:13468–13479.
- Poon IK, Chiu YH, Armstrong AJ, Kinchen JM, Juncadella IJ, Bayliss DA, and Ravichandran KS (2014) Unexpected link between an antibiotic, pannexin channels and apoptosis. *Nature* **507**:329–334.
- Pouwels SD, Zijlstra GJ, van der Toorn M, Hesse L, Gras R, Ten Hacken NH, Krysko DV, Vandenabeele P, de Vries M, van Oosterhout AJ, et al. (2016) Cigarette smoke-induced necroptosis and DAMP release trigger neutrophilic airway inflammation in mice. *Am J Physiol Lung Cell Mol Physiol* **310**:L377–L386.
- Quintana A, Schwindling C, Wenning AS, Becherer U, Rettig J, Schwarz EC, and Hoth M (2007) T cell activation requires mitochondrial translocation to the immunological synapse. *Proc Natl Acad Sci USA* **104**:14418–14423.
- Quintero IB, Araujo CL, Pulkka AE, Wirkkala RS, Herrala AM, Eskelinen EL, Jokitalo E, Hellström PA, Tuominen HJ, Hirvikoski PP, et al. (2007) Prostatic acid phosphatase is not a prostate specific target. *Cancer Res* **67**:6549–6554.
- Resta R, Yamashita Y, and Thompson LF (1998) Ecto-enzyme and signaling functions of lymphocyte CD73. *Immunol Rev* **161**:95–109.
- Ricci JE, Muñoz-Pinedo C, Fitzgerald P, Bailly-Maitre B, Perkins GA, Yadava N, Scheffler IE, Ellisman MH, and Green DR (2004) Disruption of mitochondrial function during apoptosis is mediated by caspase cleavage of the p75 subunit of complex I of the electron transport chain. *Cell* **117**:773–786.
- Robson SC, Sévigny J, and Zimmermann H (2006) The E-NTPDase family of ectonucleotidases: Structure function relationships and pathophysiological significance. *Purinergic Signal* **2**:409–430.
- Sandilos JK, Chiu YH, Chekeni FB, Armstrong AJ, Walk SF, Ravichandran KS, and Bayliss DA (2012) Pannexin 1, an ATP release channel, is activated by caspase cleavage of its pore-associated C-terminal autoinhibitory region. *J Biol Chem* **287**:11303–11311.
- Schenk B and Fulda S (2015) Reactive oxygen species regulate Smac mimetic/TNF α -induced necroptotic signaling and cell death. *Oncogene* **34**:5796–5806.
- Stagg J, Divisekera U, Duret H, Sparwasser T, Teng MW, Darcy PK, and Smyth MJ (2011) CD73-deficient mice have increased antitumor immunity and are resistant to experimental metastasis. *Cancer Res* **71**:2892–2900.
- Stagg J and Smyth MJ (2010) Extracellular adenosine triphosphate and adenosine in cancer. *Oncogene* **29**:5346–5358.
- Street SE, Walsh PL, Sowa NA, Taylor-Blake B, Guillot TS, Vihko P, Wightman RM, and Zylka MJ (2011) PAP and NT5E inhibit nociceptive neurotransmission by rapidly hydrolyzing nucleotides to adenosine. *Mol Pain* **7**:80.
- Su L, Quade B, Wang H, Sun L, Wang X, and Rizo J (2014) A plug release mechanism for membrane permeation by MLKL. *Structure* **22**:1489–1500.
- Sun L, Wang H, Wang Z, He S, Chen S, Liao D, Wang L, Yan J, Liu W, Lei X, et al. (2012) Mixed lineage kinase domain-like protein mediates necrosis signaling downstream of RIP3 kinase. *Cell* **148**:213–227.
- Tenev T, Bianchi K, Darding M, Broemer M, Langlais C, Wallberg F, Zachariou A, Lopez J, MacFarlane M, Cain K, et al. (2011) The ripoptosome, a signaling platform that assembles in response to genotoxic stress and loss of IAPs. *Mol Cell* **43**:432–448.
- Truman LA, Ford CA, Pasikowska M, Pound JD, Wilkinson SJ, Dumitriu IE, Melville L, Melrose LA, Ogden CA, Nibbs R, et al. (2008) CX3CL1/fractalkine is released from apoptotic lymphocytes to stimulate macrophage chemotaxis. *Blood* **112**:5026–5036.
- Vacchelli E, Ma Y, Baracco EE, Sistigu A, Enot DP, Pietrocola F, Yang H, Adjemian S, Chaba K, Semeraro M, et al. (2015) Chemotherapy-induced antitumor immunity requires formyl peptide receptor 1. *Science* **350**:972–978.
- Wang H, Sun L, Su L, Rizo J, Liu L, Wang LF, Wang FS, and Wang X (2014) Mixed lineage kinase domain-like protein MLKL causes necrotic membrane disruption upon phosphorylation by RIP3. *Mol Cell* **54**:133–146.
- Wang Q, Ju X, Zhou Y, and Chen K (2015) Necroptotic cells release find-me signal and are engulfed without proinflammatory cytokine production. *In Vitro Cell Dev Biol Anim* **51**:1033–1039.
- Waterhouse NJ, Goldstein JC, von Ahlsen O, Schuler M, Newmeyer DD, and Green DR (2001) Cytochrome c maintains mitochondrial transmembrane potential and ATP generation after outer mitochondrial membrane permeabilization during the apoptotic process. *J Cell Biol* **153**:319–328.
- Yamaguchi H, Maruyama T, Urade Y, and Nagata S (2014) Immunosuppression via adenosine receptor activation by adenosine monophosphate released from apoptotic cells. *eLife* **3**:e02172.
- Yegutkin GG (2008) Nucleotide- and nucleoside-converting ectoenzymes: Important modulators of purinergic signalling cascade. *Biochim Biophys Acta* **1783**:673–694.
- Yegutkin GG, Auvinen K, Karikoski M, Rantakari P, Gerke H, Elima K, Maksimov M, Quintero IB, Vihko P, Salmi M, et al. (2014) Consequences of the lack of CD73 and prostatic acid phosphatase in the lymphoid organs. *Mediators Inflamm* **2014**:485743.
- Yegutkin GG, Henttinen T, Samburski SS, Szychala J, and Jalkanen S (2002) The evidence for two opposite, ATP-generating and ATP-consuming, extracellular pathways on endothelial and lymphoid cells. *Biochem J* **367**:121–128.
- Yegutkin GG, Mikhailov A, Samburski SS, and Jalkanen S (2006) The detection of micromolar pericellular ATP pool on lymphocyte surface by using lymphoid ecto-adenylate kinase as intrinsic ATP sensor. *Mol Biol Cell* **17**:3378–3385.
- Young A, Mittal D, Stagg J, and Smyth MJ (2014) Targeting cancer-derived adenosine: new therapeutic approaches. *Cancer Discov* **4**:879–888.
- Zabielska MA, Borkowski T, Slominska EM, and Smolinski RT (2015) Inhibition of AMP deaminase as therapeutic target in cardiovascular pathology. *Pharmacol Rep* **67**:682–688.
- Zitvogel L, Apetoh L, Ghiringhelli F, and Kroemer G (2008) Immunological aspects of cancer chemotherapy. *Nat Rev Immunol* **8**:59–73.
- Zylka MJ, Sowa NA, Taylor-Blake B, Twomey MA, Herrala A, Voikar V, and Vihko P (2008) Prostatic acid phosphatase is an ectonucleotidase and suppresses pain by generating adenosine. *Neuron* **60**:111–122.

Address correspondence to: Dr. George R. Dubyak, Department of Physiology & Biophysics, School of Medicine, Case Western Reserve University, 10900 Euclid Avenue, Cleveland OH 44106. E-mail: george.dubyak@case.edu